The equilibrium alluvial river under variable flow and its channel-forming discharge

Blom, Astrid; Arkesteijn, Liselot; Chavarrias Borras, Victor; Viparelli, Enrica

Important note
To cite this publication, please use the final published version (if applicable).
Please check the document version above.

The equilibrium alluvial river under variable flow and its channel-forming discharge

Astrid Blom[1] (ID), **Liselot Arkesteijn[1]** (ID), **Víctor Chavarrías[1]** (ID), **and Enrica Viparelli[2]** (ID)

[1]Faculty of Civil Engineering and Geosciences, Delft University of Technology, Delft, Netherlands, [2]Department of Civil and Environmental Engineering, University of South Carolina, Columbia, South Carolina, USA

Correspondence to:
A. Blom,
astrid.blom@tudelft.nl

Abstract When the water discharge, sediment supply, and base level vary around stable values, an alluvial river evolves toward a mean equilibrium or graded state with small fluctuations around this mean state (i.e., a dynamic or statistical equilibrium state). Here we present analytical relations describing the mean equilibrium geometry of an alluvial river under variable flow by linking channel slope, width, and bed surface texture. The solution holds in river normal flow zones (or outside both the hydrograph boundary layer and the backwater zone) and accounts for grain size selective transport and particle abrasion. We consider the variable flow rate as a series of continuously changing yet steady water discharges (here termed an alternating steady discharge). The analysis also provides a solution to the channel-forming water discharge, which is here defined as the steady water discharge that, given the mean sediment supply, provides the same equilibrium channel slope as the natural long-term hydrograph. The channel-forming water discharge for the gravel load is larger than the one associated with the sand load. The analysis illustrates how the load is distributed over the range of water discharge in the river normal flow zone, which we term the "normal flow load distribution". The fact that the distribution of the (imposed) sediment supply spatially adapts to this normal flow load distribution is the origin of the hydrograph boundary layer. The results quantify the findings by Wolman and Miller (1960) regarding the relevance of both magnitude and frequency of the flow rate with respect to channel geometry.

1. Introduction

The flow rate and sediment load in natural streams vary widely in space and time, as precipitation and sediment supply from hillslopes and tributaries vary spatially and temporally within the basin. In general, the downstream water surface base level also changes in time due to tides, storm surge, and, on a larger time scale, sea level change.

Despite such temporal variation, the river continuously adapts through changes in planform, bed elevation, and bed surface texture and approaches its graded or equilibrium longitudinal profile [*Gilbert*, 1877; *Mackin*, 1948; *Lane*, 1955; *Ahnert*, 1994; *Buffington*, 2012; *Blom et al.*, 2016]. Following *Blom et al.* [2016], we define the graded or equilibrium river profile as the mean profile that the river approaches when flow, sediment supply, and base level vary around stable values for a long time in the absence of subsidence or uplift. The fact that a graded state in terms of channel slope and bed surface texture also develops when the flow rate, the sediment supply, and the downstream base level vary around stable values [e.g., *Pickup and Rieger*, 1979] is confirmed through laboratory experiments [*Wilcock et al.*, 2001], indirect analysis of field data [*Wilcock and DeTemple*, 2005], and numerical runs [*Parker*, 2004a; *Wong and Parker*, 2006; *Parker et al.*, 2008; *Viparelli et al.*, 2011; *Bolla Pittaluga et al.*, 2014]. This graded state is characterized by a mean state with small fluctuations around it, which is termed a statistical equilibrium or steady state equilibrium [*Chorley and Kennedy*, 1971, p. 202] or dynamic equilibrium [*De Vries*, 1993; *Ahnert*, 1994; *Zhou et al.*, 2017] and needs to be considered over a period of years or decades.

Variability of the flow rate due to flood waves is essential for, for instance, floodplain-related mechanisms [e.g., *Lauer and Parker*, 2008; *Lauer et al.*, 2016; *Viparelli et al.*, 2013; *Fleischmann et al.*, 2016] and plant colonization of exposed bars [*Tal and Paola*, 2010; *Vargas-Luna*, 2016]. Although extreme events may induce changes to the river system that moderate flows cannot [*Buffington*, 2012], for instance, the formation of new gullies, the creation of meander cutoffs, floodplain scour, and the movement of huge boulders [*Wolman and Miller*, 1960; *Pickup and Warner*, 1976; *Lenzi et al.*, 2006], flow events of moderate magnitude, which recur relatively

frequently, are more effective in transporting sediment than rare events of unusual magnitude [*Wolman and Miller*, 1960].

Various approaches have been used to formulate a representative steady water discharge that, given enough time, would produce the same channel geometry as the natural long-term hydrograph [e.g., *NEDECO*, 1959; *Prins and de Vries*, 1971; *Pickup and Warner*, 1976; *Pickup and Rieger*, 1979; *Hey*, 1996; *Emmett and Wolman*, 2001; *Copeland et al.*, 2005]. This natural long-term hydrograph is here defined as the hydrograph that covers the flow rate statistics of several years or decades. The concept of a channel-forming discharge was first introduced in the design of irrigation channels, in which the variation of the flow rate is generally limited [e.g., *Lacey*, 1930]. Application of this concept to the design, maintenance, and restoration of natural streams, which are subject to a much wider range of flow rates, initiated a search for a single value of the water discharge representative in its effect on channel geometry [*Pickup and Rieger*, 1979; *Copeland et al.*, 2005; *Gomez et al.*, 2007]. Although the terminology has not always been consistent, the following representative discharges have been proposed:

1. First is the bankfull discharge, which is the flow rate at which the channel is just filled to the top of its banks and which therefore agrees to the condition of incipient flooding [e.g., *Wolman and Leopold*, 1957; *Williams*, 1978; *Parker*, 1978a; 1978b; *Emmett and Wolman*, 2001; *Gomez et al.*, 2007; *Parker et al.*, 2007; *Phillips and Jerolmack*, 2016]. The bankfull discharge is considered morphodynamically relevant as it represents the breakpoint between processes of channel formation and floodplain formation [*Copeland et al.*, 2005] and above which the shear stress almost stops increasing with increasing discharge.

2. Second is the effective discharge, which is the water discharge at which the product of the probability density of the water discharge and the associated sediment load reaches a maximum value [e.g., *Wolman and Miller*, 1960; *Benson and Thomas*, 1966; *Andrews*, 1980; *Nash*, 1994; *Carling*, 1988; *Emmett and Wolman*, 2001; *Goodwin*, 2004].

3. Third is the discharge associated with a certain recurrence interval or a designated flood peak frequency [e.g., *Wolman and Leopold*, 1957; *Bray*, 1975; *Doyle et al.*, 2007].

4. Fourth is the formative discharge for meanders, which is the steady water discharge that provides the same meander length as the long-term hydrograph [e.g., *Benson and Thomas*, 1966; *Ackers and Charlton*, 1970], or other morphodynamic units such as bars and islands [*Surian et al.*, 2009].

5. Fifth is the slope-equivalent water discharge, which is the steady water discharge that, given the mean sediment supply, results in the same equilibrium channel slope as the long-term hydrograph (based on the approach by *De Vries* [1974, 1993], *Jansen et al.* [1979], and *Howard* [1980]) or, equivalently, the steady water discharge that for a given slope provides the same sediment flux as the long-term hydrograph [*Doyle and Shields*, 2008, their functional-equivalent discharge].

6. Sixth is the half-load discharge, which is the water discharge above and below which 50% of the total sediment load is transported [*Van Bendegom*, 1967; *Prins*, 1969; *Vogel et al.*, 2003; *Klonsky and Vogel*, 2011].

7. Seventh is the channel-forming flood, which is the average of all water discharges at which gravel is mobilized weighted by the probability of their occurrence [*Phillips and Jerolmack*, 2016].

Yet despite the efforts to find an estimate of a single representative discharge, it has also been realized that no single steady discharge can affect all characteristics of channel geometry in a similar manner as the varying flow rate [*NEDECO*, 1959; *Prins*, 1969; *Prins and de Vries*, 1971; *De Vries*, 1971, 1993; *Biedenharn et al.*, 2008]. This calls for a precise definition of the type of representative discharge one is considering [*Prins and de Vries*, 1971]: exactly what morphodynamic aspect should be reproduced by the representative discharge?

Our objective is to determine relations linking the equilibrium channel slope, channel width, and bed surface texture under variable flow and to provide a definition of the slope-equivalent or channel-forming discharge. To this end, we follow the analysis introduced by *De Vries* [1974, pp. 31–32], which is more accessible in *Jansen et al.* [1979, pp. 119–121], *De Vries* [1993], *Howard* [1980], and *Doyle and Shields* [2008]. We extend their analysis to mixed-size sediment conditions. Our analysis also is an extension of the *Blom et al.* [2016] equations for the equilibrium geometry of an alluvial river to a variable flow rate.

In the next section we explain how we treat the variable flow rate in our analysis and propose relations to determine the mean sediment load under a variable flow rate with temporally constant statistics. In section 3 we describe the equilibrium river geometry under variable flow and unisize sediment conditions. To this end, we consider a variable flow rate that at each time is governed by steady flow. We extend this analysis to mixed sediment by accounting for the mechanisms of grain size selective transport and particle abrasion in section 4. In section 5 we validate the analytical model by comparing its results for the equilibrium river geometry
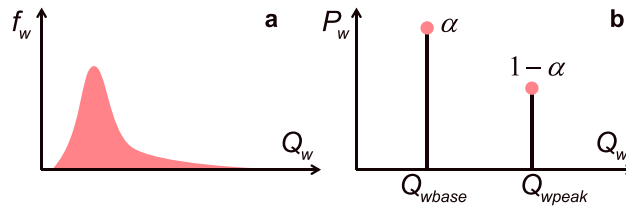
Figure 1. Statistics of the flow rate expressed by (a) a probability density function (PDF) of water discharge for an arbitrary long-term hydrograph and (b) the probabilities of a two-modes water discharge.

to those of two numerical time-marching models, one based on the backwater equation and one on the *Saint-Venant* [1871] equations. We discuss channel response to changing boundary conditions through slope and width adjustment in section 6. In section 7 we illustrate how the analytical model allows for predicting the relative contribution of the long-term range of flow rate values to transporting the (gravel and sand) load, which we term the "normal flow load distribution". In section 8 we address the differences between the slope-equivalent discharge and the effective discharge defined by *Wolman and Miller* [1960].

2. Hydrograph Treatment and Formulations for the Mean Load

As we focus on a dynamic or statistical steady state, we model the variability of the water discharge, Q_w (m³/s), in terms of a changing flow rate of which the statistics are temporally constant and expressed by the probability density function (PDF) of water discharge, $f_w(Q_w)$ (s/m³) [*Wolman and Miller*, 1960].

Now let us consider the arbitrary probability density function of water discharge shown in Figure 1a. The integral of the PDF by definition equals unity. The expected or mean sediment load, $E[Q]$ or $\bar{Q}$, equals

$$E[Q] \equiv \bar{Q} = \int_0^\infty Q(Q_w)f_w(Q_w)\mathrm{d}Q_w \tag{1}$$

which is equivalent to equation (3.3–31) in *Jansen et al.* [1979], equation (2–31) in *De Vries* [1993], and equation (4) in *Doyle and Shields* [2008]. The bar indicates the fact that we average over a significant period and hence deal with the expected or mean value.

For illustration purposes we simplify the PDF of water discharge to a discrete distribution with two modes: a base flow rate, $Q_{w\,\text{base}}$, and a peak flow rate, $Q_{w\,\text{peak}}$ (Figure 1b). The probability that base flow occurs is denoted by α (–), and for a two modes case the probability that peak flow occurs, by definition, equals $1 - \alpha$. For this two-modes distribution of the flow rate equation (1) is simplified to

$$\bar{Q} = \alpha Q_{\text{base}} + (1 - \alpha)Q_{\text{peak}} \tag{2}$$

where the capacity-based sediment load under base and peak flow, Q_{base} and Q_{peak}, are defined as $Q(Q_{w\,\text{base}})$ and $Q(Q_{w\,\text{peak}})$, respectively.

Similarly, under conditions with two sediment modes, gravel and sand, the mean gravel and sand load, $\bar{Q}_g$ and $\bar{Q}_s$, are equal to

$$\bar{Q}_g = \int_0^\infty Q_g(Q_w)f_w(Q_w)\mathrm{d}Q_w \tag{3}$$

$$\bar{Q}_s = \int_0^\infty Q_s(Q_w)f_w(Q_w)\mathrm{d}Q_w \tag{4}$$

where the subscripts *g* and *s* indicate gravel and sand, respectively. Equations (3) and (4) are simplified to

$$\bar{Q}_g = \alpha Q_{g\,\text{base}} + (1 - \alpha)Q_{g\,\text{peak}} \tag{5}$$

$$\bar{Q}_s = \alpha Q_{s\,\text{base}} + (1 - \alpha)Q_{s\,\text{peak}} \tag{6}$$

for the two-modes water discharge regime of Figure 1b.

3. Equilibrium River Geometry for Unisize Sediment

To describe the equilibrium river geometry under a variable flow rate, we first consider the case of unisize sediment. For that purpose we combine equation (1) or (2) with a formulation for the sediment load as a function of the flow rate. After listing our simplifications in section 3.1, we apply a power law load relation
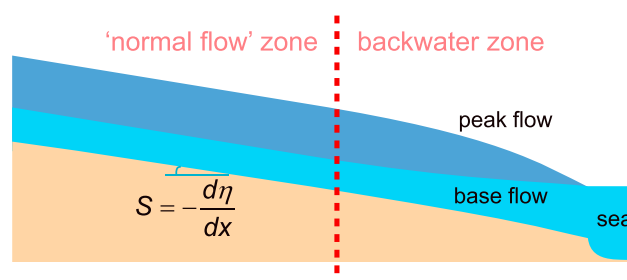
Figure 2. Schematic of variable flow under a constant base level in a mildly sloping river: the "normal flow" zone and the backwater zone. Although the figure shows one normal flow zone and one backwater zone, a river typically consists of multiple backwater zones and normal flow zones. The proposed formulations for the equilibrium river geometry under variable flow are valid in river normal flow zones.

which leads to an explicit analytical solution to the equilibrium river geometry (section 3.2), as well as more complex load relations leading to implicit analytical solutions (section 3.3).

3.1. Simplifications and the "Alternating Steady Flow" Assumption

We make a number of simplifying assumptions to obtain an analytical solution to the equilibrium river geometry: (1) our model is one-dimensional; (2) we neglect subsidence and uplift, base level change, and delta outbuilding; (3) we assume a rectangular cross section of width, B (m), and do not distinguish between flow through the main channel and the floodplains; (4) we consider a relatively wide channel, which implies that we can assume that the hydraulic radius equals the flow depth, H (m); (5) we assume hydrostatic pressure in the water column; (6) we assume the nondimensional friction coefficient, C_f (−), to be independent of the local flow parameters and the surface texture; (7) we neglect changes in sediment porosity; (8) we consider bed material load only (i.e., bed load and suspended bed material load [*Paola*, 2001; *Church*, 2006]); and (9) we neglect the spatial lag in the adaptation to capacity-based transport rates [*Phillips and Sutherland*, 1989].

A high precipitation rate and the associated temporally increased flow rate lead to a flood wave that is advected downstream while diffusing. Consequently, the water discharge varies also spatially, which induces small temporal change in bed elevation. The fact that bed elevation change under a varying flow rate is small can also be explained as follows. In general, the time scale of change in channel slope is much larger than that of the flow rate [*Mackin*, 1948; *De Vries*, 1974; *Jansen et al.*, 1979; *Howard*, 1980, 1982; *De Vries*, 1993]. In other words, there is insufficient time for the channel slope to adjust to short-term changes in the flow rate. Furthermore, any change in slope due to the variable flow rate starts at the domain boundaries. This reasoning is confirmed by the analyses of *Parker et al.* [2008], *Viparelli et al.* [2011], and *An et al.* [2017a, 2017b].

In the lower course of a river, the flood wave is typically longer than in its upper course, as it has diffused while migrating downstream. Here we assume that the flood wave is infinitely long and propagates infinitely fast, which implies that it does not dampen. Thus, although we do consider the temporal variability of the flow rate, we do not consider the dynamics of a flood wave. In other words, we assume that the flow is steady for each value of the flow rate and term this an alternating steady flow.

We divide the fluvial reach into two zones: backwater zones that are controlled by a downstream water surface base level and normal flow zones where the flow is not affected by the base level (Figure 2). A "river normal flow zone" is defined as a reach where the flow can be reasonably approximated as uniform or normal, even under a variable flow rate. This implies that for all flow rates the friction slope is more or less equal to the bed slope and that, by definition, bed elevation changes are zero. Although Figure 2 shows one normal flow zone and one backwater zone, a river typically consists of multiple backwater and normal flow zones, yet backwater effects may prevail such that a strictly normal flow zone is absent. The analysis presented in this paper is applicable to river normal flow zones only, and therefore we consider a static equilibrium state.

3.2. An Explicit Analytical Model

We first apply a power law load relation without a threshold for significant transport [e.g., *Engelund and Hansen*, 1967; *Parker*, 1990a, 1990b; *Syvitski et al.*, 2000; *Emmett and Wolman*, 2001; *Wilcock and Crowe*, 2003; *Goodwin*, 2004; *Barry et al.*, 2004, 2007; *Doyle and Shields*, 2008; *Houssais et al.*, 2015], which reflects *Einstein*, 's [1950] probabilistic philosophy regarding the nature of sediment transport.

We now summarize existing power law load relations into a simple generalized load relation for unisize sediment:

$$W^* = c \left(\frac{D}{D_{\text{ref}}} \right)^r \tau^{*w} \tag{7}$$

where W^* (−) denotes the nondimensional sediment transport rate ($W^* = q^*/\tau^{*3/2}$ with q^* denoting the non-dimensional Einstein transport number; see *Parker* [2004b] or Appendix A), τ^* (−) is the grain-related Shields stress or the Shields stress associated with skin friction, c (−), w (−), and r (−) are constants, and D (m) is the representative grain size of the sediment. We introduce the parameter D_{ref} (m) to nondimensionalize the right-hand term of equation (7) ($D_{ref} = 0.001$ m). Equation (7) is simplified to the *Engelund and Hansen* [1967] load relation by setting $w = 1$, $r = 0$, and $c = 0.05C_f^{3/2}/C_{fs}^{5/2}$ where C_{fs} (−) denotes the nondimensional skin friction coefficient. Appendix A provides more detailed information on the generalized load relation.

We apply equation (7) to estimate the sediment transport rates at base and peak flow rates, Q_{base} and Q_{peak}, that are required in equation (2). To this end, we combine the formulation for the sediment load, equation (7) or (A3), with the continuity equation for the flow ($Q_w = BUH$ with U (m/s) denoting the mean flow velocity), and we use the normal flow equation, $H = (C_f Q_w^2/(SB^2 g))^{1/3}$, to eliminate the flow depth H:

$$Q = \frac{G}{D^w}\frac{(D/D_{ref})^r}{B^{2w/3}}\left(\frac{gSQ_w}{C_f}\right)^{(2w+3)/3}$$

(8)

where S (−) denotes channel slope, g (m/s²) the gravitational acceleration, and G is a constant in the load relation (equation (A3b)).

We use equation (8) to replace Q_{base} and Q_{peak} in equation (2) and assume that the equilibrium channel slope, S, does not vary with the varying flow rate (section 3.1). We then find the following equation for the equilibrium channel slope under variable flow in a reach governed by normal flow:

$$S = \frac{C_f B^{2w/(2w+3)}}{gQ_{w\,dom}}\left(\frac{D^w}{G}\frac{\bar{Q}}{(D/D_{ref})^r}\right)^{3/(2w+3)}$$

(9)

where the slope-equivalent discharge, $Q_{w\,dom}$, for the case of a two modes discharge is given by

$$Q_{w\,dom} = \left(\alpha Q_{w\,base}^{(2w+3)/3} + (1-\alpha)Q_{w\,peak}^{(2w+3)/3}\right)^{3/(2w+3)}$$

(10)

We generalize equation (10) to the case of the arbitrary PDF of water discharge in Figure 1a:

$$Q_{w\,dom} = \left[\int_0^\infty Q_w^{(2w+3)/3} f_w\left(Q_w\right) \mathrm{d}Q_w\right]^{3/(2w+3)}$$

(11)

which is an elaborated form of the functional-equivalent discharge defined by *Doyle and Shields* [2008, equation (6)].

The current analysis conveniently provides a definition of the slope-equivalent or channel-forming discharge, $Q_{w\,dom}$, for conditions with varying flow. This representative water discharge is the steady water discharge that, given the mean sediment supply, results in the same equilibrium channel slope as the natural long-term hydrograph.

Naturally, under variable flow the flow depth depends on the flow stage at time t or discharge mode Q_w and, outside backwater zones (Figure 2), is found by combining equation (9) with the normal flow equation:

$$H(t) = \frac{Q_w(t)^{2/3}Q_{w\,dom}^{1/3}}{B^{(2w+2)/(2w+3)}}\left(\frac{G}{D^w}\frac{(D/D_{ref})^r}{\bar{Q}}\right)^{1/(2w+3)}$$

(12)

The flow velocity at time t, $U(t)$, is found by combining $Q_w = BUH$ with equation (12):

$$U(t) = \left(\frac{Q_w(t)}{Q_{w\,dom}}\right)^{1/3}\left(\frac{D^w}{G}\frac{\bar{Q}}{B(D/D_{ref})^r}\right)^{1/(2w+3)}$$

(13)

Table 1. Overview of Equations for the Equilibrium River Geometry Under Variable Flow in a River Normal Flow zone[a]

	Generalized Load Relation (GR) (provided that $w_g = w_s = w$)	Engelund and Hansen (1967) (EH)
Channel-Forming Discharge	$Q_{w\,dom} = \left[\int_0^\infty Q_w^{(2w+3)/3} f_w(Q_w)\,dQ_w\right]^{3/(2w+3)}$	$Q_{w\,dom} = \left[\int_0^\infty Q_w^{5/3} f_w(Q_w)\,dQ_w\right]^{3/5}$
	$Q_{w\,dom} = \left(\alpha Q_{w\,base}^{(2w+3)/3} + (1-\alpha)Q_{w\,peak}^{(2w+3)/3}\right)^{3/(2w+3)}$	$Q_{w\,dom} = \left(\alpha Q_{w\,base}^{5/3} + (1-\alpha)Q_{w\,peak}^{5/3}\right)^{3/5}$

UNISIZE	*BLOCK 1*	*BLOCK 2*
	$S = \dfrac{C_f B^{2w/(2w+3)}}{g Q_{w\,dom}}\left(\dfrac{D^w}{G}\dfrac{\bar{Q}}{(D/D_{ref})^r}\right)^{3/(2w+3)}$	$S = \dfrac{C_f B^{2/5}}{g Q_{w\,dom}}\left(\dfrac{D}{G_{EH}}\bar{Q}\right)^{3/5}$
	$H(t) = \dfrac{Q_w(t)^{2/3}Q_{w\,dom}^{1/3}}{B^{(2w+2)/(2w+3)}}\left(\dfrac{G}{D^w}\dfrac{(D/D_{ref})^r}{\bar{Q}}\right)^{1/(2w+3)}$	$H(t) = \dfrac{Q_w(t)^{2/3}Q_{w\,dom}^{1/3}}{B^{4/5}}\left(\dfrac{G_{EH}}{D}\dfrac{1}{\bar{Q}}\right)^{1/5}$
	$U(t) = \left(\dfrac{Q_w(t)}{Q_{w\,dom}}\right)^{1/3}\left(\dfrac{D^w}{G}\dfrac{\bar{Q}}{B(D/D_{ref})^r}\right)^{1/(2w+3)}$	$U(t) = \left(\dfrac{Q_w(t)}{Q_{w\,dom}}\right)^{1/3}\left(\dfrac{D}{G_{EH}}\dfrac{\bar{Q}}{B}\right)^{1/5}$

MIXED	*BLOCK 3*	*BLOCK 4*
	$S = \dfrac{C_f B^{2w/(2w+3)}}{g Q_{w\,dom}}\left(\dfrac{D_s^w \mu}{G}\dfrac{\bar{Q}}{(D_g/D_{ref})^r}\right)^{3/(2w+3)}$	$S = \dfrac{C_f B^{2/5}}{g Q_{w\,dom}}\left(\dfrac{D_s \mu}{G_{EH}}\bar{Q}\right)^{3/5}$
	$F = \dfrac{1}{\mu}\left(\dfrac{D_g}{D_s}\right)^w \bar{p}_g$	$F = \dfrac{1}{\mu}\dfrac{D_g}{D_s}\bar{p}_g$
	$H(t) = \dfrac{Q_w(t)^{2/3}Q_{w\,dom}^{1/3}}{B^{(2w+2)/(2w+3)}}\left(\dfrac{G}{D_s^w \mu}\dfrac{(D_g/D_{ref})^r}{\bar{Q}}\right)^{1/(2w+3)}$	$H(t) = \dfrac{Q_w(t)^{2/3}Q_{w\,dom}^{1/3}}{B^{4/5}}\left(\dfrac{G_{EH}}{D_s \mu}\dfrac{1}{\bar{Q}}\right)^{1/5}$
	$U(t) = \left(\dfrac{Q_w(t)}{Q_{w\,dom}}\right)^{1/3}\left(\dfrac{D_s^w \mu}{G}\dfrac{\bar{Q}}{B(D_g/D_{ref})^r}\right)^{1/(2w+3)}$	$U(t) = \left(\dfrac{Q_w(t)}{Q_{w\,dom}}\right)^{1/3}\left(\dfrac{D_s \mu}{G_{EH}}\dfrac{\bar{Q}}{B}\right)^{1/5}$
	$\mu = \left(\dfrac{D_g}{D_s}\right)^r\left(1-\bar{p}_g\right) + \left(\dfrac{D_g}{D_s}\right)^w \bar{p}_g$	$\mu = 1 - \bar{p}_g + \dfrac{D_g}{D_s}\bar{p}_g$

MIXED AND ABRASION	*BLOCK 5*	*BLOCK 6*
	$S = \dfrac{C_f B^{2w/(2w+3)}}{g Q_{w\,dom}}\left(\dfrac{D_s^w \mu}{G}\dfrac{\bar{Q}_0}{(D_{gx}/D_{ref})^r}\right)^{3/(2w+3)}$	$S = \dfrac{C_f B^{2/5}}{g Q_{w\,dom}}\left(\dfrac{D_s \mu}{G_{EH}}\bar{Q}_0\right)^{3/5}$
	$F = \dfrac{1}{\mu}\left(\dfrac{D_{gx}}{D_s}\right)^w \bar{p}_{g0}e^{-x_\kappa^*}$	$F = \dfrac{1}{\mu}\dfrac{D_{gx}}{D_s}\bar{p}_{g0}e^{-x_\kappa^*}$
	$H(t) = \dfrac{Q_w(t)^{2/3}Q_{w\,dom}^{1/3}}{B^{(2w+2)/(2w+3)}}\left(\dfrac{G}{D_s^w \mu}\dfrac{(D_{gx}/D_{ref})^r}{\bar{Q}_0}\right)^{1/(2w+3)}$	$H(t) = \dfrac{Q_w(t)^{2/3}Q_{w\,dom}^{1/3}}{B^{4/5}}\left(\dfrac{G_{EH}}{D_s \mu}\dfrac{1}{\bar{Q}_0}\right)^{1/5}$
	$U(t) = \left(\dfrac{Q_w(t)}{Q_{w\,dom}}\right)^{1/3}\left(\dfrac{D_s^w \mu}{G}\dfrac{\bar{Q}_0}{B(D_{gx}/D_{ref})^r}\right)^{1/(2w+3)}$	$U(t) = \left(\dfrac{Q_w(t)}{Q_{w\,dom}}\right)^{1/3}\left(\dfrac{D_s \mu}{G_{EH}}\dfrac{\bar{Q}_0}{B}\right)^{1/5}$
	$\mu = \left(\dfrac{D_{gx}}{D_s}\right)^r\left(1-\bar{p}_{g0}+k_{ss}\bar{p}_{g0}(1-e^{-x_\kappa^*})\right) + \left(\dfrac{D_{gx}}{D_s}\right)^w \bar{p}_{g0}e^{-x_\kappa^*}$	$\mu = 1 - \bar{p}_{g0} + k_{ss}\bar{p}_{g0}\left(1-e^{-x_\kappa^*}\right) + \dfrac{D_{gx}}{D_s}\bar{p}_{g0}e^{-x_\kappa^*}$

[a]The set of equations in Block 5 is the fundamental set of equations: the equations in the other blocks can be found by simplifying the ones in Block 5. For the case of a single steady discharge the equations in Block 6 reduce to the ones derived by *Blom et al.* [2016].

The equations governing the equilibrium river geometry under unisize sediment conditions are summarized in Block 1 of Table 1. Applying the *Engelund and Hansen* [1967] load relation, these equations reduce to the ones listed in Block 2. The slope-equivalent discharges in equations (10) and (11) are simplified to the ones listed in the upper right-hand corner of Table 1.

The equations for the equilibrium channel slope and flow depth under a variable flow rate are similar to the *Blom et al.* [2016] equations obtained for the constant water discharge case. Noteworthy is the resulting definition of a slope-equivalent or channel-forming discharge. The slope-equivalent discharge is larger than the mean water discharge, which is due to the nonlinear relation between water discharge and the sediment transport rate.

The equations provide an order of magnitude of the relative change that can be expected on the long term if one of the controls changes with time. Let us consider an engineered river with fixed banks in which the mean

sediment supply decreases by a factor 2 (for instance, due to a dam). According to the *Engelund and Hansen* [1967] load relation and assuming that the initial state is an equilibrium state, equation (9) tells us that the slope decreases of the order of 30% eventually.

Equation (9) also illustrates how in the equilibrium state the channel slope, S, scales with

$$S \propto \frac{(D^{w-r}\bar{Q})^{3/(2w+3)}}{Q_{w\,dom}} \tag{14}$$

($w = 1$ and $r = 0$ if applying the *Engelund and Hansen* [1967] load relation) which is very similar to the *Lane* [1955] relation for channel slope:

$$S \propto \frac{DQ}{Q_w} \tag{15}$$

where here Q and Q_w are representative values of the sediment and water discharge. Yet formulations somewhat different from equation (14) will be found when applying other load relations.

Slope adjustment arises through reach-scale aggradation/degradation or changes in channel sinuosity [e.g., *Buffington*, 2012]. In cases where the river responds to changes in the boundary conditions through width adjustment rather than slope adjustment [*Howard*, 1980], one may impose channel slope, S, and use equation (9) to compute the equilibrium channel width, B. Alternatively, in cases where the river responds to changes through a combination of slope and width adjustment, one can combine the current formulation for the equilibrium channel slope in equations (9) with a closure relation and solve for both the equilibrium channel slope and width. We will address this topic in more detail in sections 4.2 and 6.

3.3. An Implicit Analytical Model

After using the power law load relation that has led to an explicit solution to the equilibrium river geometry, we here apply more complex load relations, for instance, one with a threshold value for significant transport. This leads to implicit analytical solutions to the equilibrium river geometry. Following the same procedure as described in the previous section, yet using the load relation by, for instance, *Meyer-Peter and Müller* [1948] or *Fernandez-Luque and Van Beek* [1976], equation (8) is replaced by

$$Q = aB\sqrt{RgDD}\left[\max\left(0, \left(\frac{Q_w^2 S^2}{C_f^2 B^2 g}\right)^{1/3} \frac{C_{fs}}{RD} - \tau_c^*\right)\right]^b \tag{16}$$

where R (−) is the submerged specific gravity ($R = (\rho_s - \rho)/\rho$ in which ρ_s (kg/m³) and ρ (kg/m³) are the sediment and water density, respectively). According to *Meyer-Peter and Müller* [1948], the values of the nondimensional constants in the load relation are $a = 8$, $b = 1.5$, and $\tau_c^* = 0.047$, and according to *Fernandez-Luque and Van Beek* [1976], $a = 5.7$, $b = 1.5$, and $\tau_c^* = 0.037 \sim 0.0455$. The maximization function is included to indicate that the excess Shields stress cannot be negative. As an example, we apply equation (16) to elaborate on the base and peak flow sediment transport rates in equation (2):

$$\begin{aligned}
\frac{\bar{Q}}{aB\sqrt{RgDD}} = \alpha &\left[\max\left(0, \left(\frac{Q_{w\,base}^2 S^2}{C_f^2 B^2 g}\right)^{1/3} \frac{C_{fs}}{RD} - \tau_c^*\right)\right]^b \\
+ (1-\alpha) &\left[\max\left(0, \left(\frac{Q_{w\,peak}^2 S^2}{C_f^2 B^2 g}\right)^{1/3} \frac{C_{fs}}{RD} - \tau_c^*\right)\right]^b
\end{aligned} \tag{17}$$

and solve equation (17) iteratively for the equilibrium channel slope, S, or channel width, B, depending on the unknown variable in the equation, or add a closure relation and solve for both channel slope and channel width. Equation (17) is easily generalized to account for any number of discharge values or an arbitrary PDF of water discharge.

The slope-equivalent discharge, $Q_{w\,dom}$, which is the steady water discharge that yields the equilibrium channel slope S or channel width B computed from equation (17), can be determined from

$$\frac{\bar{Q}}{aB\sqrt{RgDD}} = \left[\max\left(0, \left(\frac{Q_{w\,dom}^2 S^2}{C_f^2 B^2 g}\right)^{1/3} \frac{C_{fs}}{RD} - \tau_c^*\right)\right]^b \tag{18}$$

The implicit character of the solution procedure here arises from the threshold for significant transport. This procedure can be applied to any existing load relation and will be validated in section 5. Before doing so, we will extend the model to mixed-size sediment conditions.

4. Equilibrium River Geometry for Mixed Sediment

4.1. Simplifications

In this section we extend the model of the equilibrium river geometry under variable yet normal flow to conditions with mixed-size sediment. Following *Ferguson* [2003], *Gasparini et al.* [2004], and *Blom et al.* [2016], we limit our analysis to sediment mixtures characterized by two distinct modes, gravel and sand. Besides the assumptions listed in section 3.1, the mixed-size sediment model consists of a number of additional simplifying assumptions [*Blom et al.*, 2016]: (1) all gravel particles entering the reach at the upstream end have the same grain size (and the same holds for sand); (2) all sediment arrives from upstream through fluvial sediment transport; (3) only gravel particles abrade, which implies that the gravel size gradually decreases with streamwise coordinate x (m), expressed by the symbol D_{gx} (m), and the sand diameter D_s (m) is constant; and (4) the products of abrasion are sand and silt, and the fraction of abrasion product that is sand (versus silt), k_{ss} (−), is imposed.

4.2. An Explicit Analytical Model

Analogous to the unisize sediment case, we first apply a generalized power law load relation to the mixed-sediment case:

$$W_i^* = c \left(\frac{D_i}{D_{\text{ref}}} \right)^r \tau_i^{*w_i} \tag{19}$$

where W_i^* (−) denotes the nondimensional sediment transport rate of grain size fraction i (here limited to either gravel or sand), D_i (m) the representative grain size of size fraction i, the coefficient w_i (−) a size fraction dependent parameter, and τ_i^* (−) is the grain-related Shields stress associated with size fraction i. Appendix B provides more detailed information on this generalized load relation.

As the transport relation in equation (19) does not include a threshold for significant transport, hiding effects cannot be accounted for through adjusting the critical Shields stress, yet the exponents r and w_i can be adjusted to modify the grain size selectivity of the load relation. Grain size selectivity increases with increasing values of $w_i - r$. Varying w_i between the grain size classes i also adjusts the grain size selectivity. The load relation is independent of grain size if $w_i = r$. It reduces to the fractional form of the *Engelund and Hansen* [1967] load relation applied by *Blom et al.* [2016] through setting $w_i = 1$, $r = 0$, and $c = 0.05 C_f^{3/2}/C_{fs}^{5/2}$.

We apply the *Hirano* [1971] active layer equation to describe the conservation of mass of gravel and sand at the bed surface [*Ribberink*, 1987; *Parker*, 1991; *Stecca et al.*, 2014, 2016]. Following *Blom et al.* [2016], we add abrasion-related terms to the *Hirano* [1971] active layer equation. Under graded or equilibrium conditions we can simplify these conservation equations for the gravel and sand mass to [*Blom et al.*, 2016]

$$\bar{Q}_g = \bar{p}_{g0} \bar{Q}_0 e^{-x_\kappa^*} \tag{20}$$

$$\bar{Q}_s = \bar{Q}_0 - \bar{p}_{g0} \bar{Q}_0 + k_{ss} \bar{p}_{g0} \bar{Q}_0 \left(1 - e^{-x_\kappa^*} \right) \tag{21}$$

where x_κ^* (−) denotes the nondimensional streamwise coordinate: $x_\kappa^* = \kappa \beta (x - x_0)$ with the constant β (1/m) denoting the abrasion coefficient and κ (-) is defined as $\kappa = 1 + F$ where F (−) denotes the volume fraction content of gravel at the bed surface. This implies $1 \leq \kappa \leq 2$. For simplicity *Blom et al.* [2016] assume κ to be constant, which implies that κ (just as β) is independent of x. Subscript 0 indicates the upstream end of the considered reach. $\bar{p}_g$ (−) is the mean gravel content in the sediment supply ($\bar{p}_g = \bar{Q}_g/\bar{Q}$ and $\bar{Q} = \bar{Q}_g + \bar{Q}_s$).

Equations (20) and (21) are not just the steady version of the *Hirano* [1971] active layer equation with added abrasion terms [*Blom et al.*, 2016] but also the steady version of vertically continuous sediment conservation models [e.g., *Parker et al.*, 2000; *Blom*, 2008; *Viparelli et al.*, 2017] with added abrasion terms. The current analysis is therefore not restricted to the application of the *Hirano* [1971] active layer equation.

If we neglect gravel particle abrasion, equations (20) and (21) simplify to $\bar{Q}_g = \bar{p}_{g0} \bar{Q}_0 = \bar{Q}_{g0}$ and $\bar{Q}_s = \bar{Q}_{s0}$, which implies that the local gravel and sand load are equal to the gravel and sand supply at the upstream end of the reach. We retain the effects of abrasion in our subsequent analysis. Under conditions with abrasion the equilibrium river longitudinal profile is concave upward and, as such, not governed by strictly normal

flow [*Blom et al.*, 2016]. Yet the associated streamwise change is small enough to assume that normal flow conditions hold.

Analogous to the procedure used to derive equation (8) or (16), we first apply equation (19) or (B3) to predicting the gravel and sand load; we then combine the resulting equations with the continuity equation for the flow and the normal flow equation, and we derive the following relations for the gravel and sand load:

$$Q_g = \frac{F}{B^{2w_g/3}} \frac{(D_{gx}/D_{ref})^r G_g}{D_{gx}^{w_g}} \left(\frac{gSQ_w}{C_f} \right)^{(2w_g+3)/3} \tag{22}$$

$$Q_s = \frac{(1-F)}{B^{2w_s/3}} \frac{(D_s/D_{ref})^r G_s}{D_s^{w_s}} \left(\frac{gSQ_w}{C_f} \right)^{(2w_s+3)/3} \tag{23}$$

where G_g and G_s are gravel and sand related constants in the load relation defined in equation (B4) and w_g and w_s are gravel and sand related constants.. Besides assuming changes in bed elevation due to the varying flow to be small, we also assume temporal changes in surface texture to be small. This assumption is justified by the findings of *Parker and Klingeman* [1982], *Parker et al.* [1982b], *Wilcock et al.* [2001], *Parker* [2004a], *Wilcock and DeTemple* [2005], *Parker et al.* [2008], *Ferrer-Boix and Hassan* [2015], and *Litty and Schlunegger* [2016].

We apply equations (22) and (23) to compute the gravel and sand load during peak flow, $Q_{g\,peak}$ and $Q_{s\,peak}$, and base flow, $Q_{g\,base}$ and $Q_{s\,base}$. For reaches unaffected by backwater effects, equations (5) and (6) yield

$$\bar{Q}_g = \frac{F}{B^{2w_g/3}} \frac{(D_{gx}/D_{ref})^r G_g}{D_{gx}^{w_g}} \left(\frac{gSQ_{w\,dom}}{C_f} \right)^{(2w_g+3)/3} \tag{24}$$

$$\bar{Q}_s = \frac{1-F}{B^{2w_s/3}} \frac{(D_s/D_{ref})^r G_s}{D_s^{w_s}} \left(\frac{gSQ_{w\,dom}}{C_f} \right)^{(2w_s+3)/3} \tag{25}$$

where $Q_{w\,dom}$ is given by equation (10) and, for the arbitrary PDF of flow rate in Figure 1a, by equation (11).

The combination of equations (24) and (25) with equations (20) and (21) while assuming the coefficient w_i to be independent of grain size ($w_g = w_s = w$ and so $G_g = G_s = G$) yields two equations describing the relation between the equilibrium channel slope, S, channel width, B, and surface gravel fraction, F:

$$S = \frac{C_f B^{2w/(2w+3)}}{gQ_{w\,dom}} \left(\frac{D_s^w \mu}{G} \frac{\bar{Q}_0}{(D_{gx}/D_{ref})^r} \right)^{3/(2w+3)} \tag{26}$$

$$F = \frac{1}{\mu} \left(\frac{D_{gx}}{D_s} \right)^w \bar{p}_{g0} e^{-x_\kappa^*} \tag{27}$$

where

$$\mu = \left(\frac{D_{gx}}{D_s} \right)^r \left(1 - \bar{p}_{g0} + k_{ss}\bar{p}_{g0}(1 - e^{-x_\kappa^*}) \right) + \left(\frac{D_{gx}}{D_s} \right)^w \bar{p}_{g0} e^{-x_\kappa^*} \tag{28}$$

Combining the equation for the channel slope with the normal flow equation and the continuity equation for the flow yields the formulations for the flow depth and flow velocity at time t or discharge mode Q_w. We have summarized the resulting formulations in Block 5 in Table 1, and, for the *Engelund and Hansen*, 1967 load relation, in Block 6 of Table 1. The resulting equations without the effects of gravel particle abrasion ($\beta = 0$) are listed in Blocks 3 and 4. For the case of a single steady discharge, the equations in Block 6 of Table 1 reduce to the equations derived by *Blom et al.* [2016].

There is a drawback to assuming the coefficient w_i to be independent of grain size ($w_g = w_s = w$), which also holds for the fractional form of the Engelund and Hansen load relation. The assumption implies that, although sand is more mobile than gravel and the load is finer than the bed surface (i.e., the sediment transport is grain size selective), the predicted load does not coarsen with increasing Shields stress. The fact that the sediment load coarsens with increasing Shields stress and that its grain size distribution becomes closer to the one of the bed surface is shown in field cases [*Kuhnle*, 1992; *Kuhnle and Willis*, 1992; *Wathen et al.*, 1995] and in laboratory experiments [*Van der Scheer et al.*, 2002, Figure 7.1]. Despite this simplification, the resulting explicit equations describing the equilibrium river geometry provide useful insight on the relation among the equilibrium channel slope, channel width, and surface texture.

Another yet related consequence of the assumption that w_i is independent of grain size is the fact that the resulting slope-equivalent discharge, $Q_{w\,dom}$, is not affected by the grain size class. In the next section we will illustrate that generally the slope-equivalent or channel-forming discharge does depend on the grain size fraction.

Just as in the analysis for a constant flow rate [*Blom et al.*, 2016], we find one equilibrium state for engineered rivers where the channel width is fixed. Such an engineered river responds to changes in boundary conditions through changes in channel slope and bed surface texture. Yet natural streams respond to changes in boundary conditions through changes in channel slope, surface texture, and channel width [*Howard*, 1980], and in that case there is a range of equilibrium states for which the channel is able to transport the load supplied from above.

In engineered rivers where the channel width cannot adjust, it is relatively straightforward to apply the presented formulations. When applying them to natural streams, two strategies can be followed to formulate a closure relation: (1) one can introduce a closure relation linking, for instance, channel width to other parameters, or (2) depending on the available data and the particular field conditions, one can solve equations (26) and (27) for two unknown parameters. For instance, we can impose the channel slope rather than the channel width, which may be a suitable option in those cases where the time scale of slope adjustment is much larger than the time scale of width adjustment [*Howard*, 1980; *Mosselman*, 2009]. For such cases we rewrite equation (9) to find a formulation for the equilibrium channel width, B:

$$B = \left(\frac{G}{D_s^w \mu} \frac{(D_{gx}/D_{ref})^r}{\bar{Q}_0} \right)^{3/2w} \left(\frac{gSQ_{w\,dom}}{C_f} \right)^{(2w+3)/2w} \tag{29}$$

The fact that channel width increases with increasing flow rate is confirmed by many authors [e.g., *Leopold and Maddock*, 1953; *Dade et al.*, 2011]. It is, however, not straightforward to compare equation (29) with empirical relations for the channel width [e.g., *Parker et al.*, 2007; *Biedenharn et al.*, 2008; *Li et al.*, 2015], as the list of included variables differs largely. We will address the topic of channel response through width adjustment in further detail in section 6.

4.3. An Implicit Analytical Model

For a sediment transport relation that (a) contains a threshold below which transport is negligible, (b) contains a hiding coefficient, or (c) is a conditional function [e.g., *Wilcock and Crowe*, 2003], we can only implicitly express channel slope or width and bed surface texture and need to iteratively find their solutions. We here provide the implicit formulations for a load relation with a threshold for significant transport yet for clarity without a hiding coefficient. For two discharge modes, the mean gravel load, $\bar{Q}_g$, and the mean sand load, $\bar{Q}_s$, in equations (5) and (6) yield

$$\frac{\bar{Q}_g}{aB\sqrt{RgD_g}D_gF} = \alpha \left[\max\left(0, \left(\frac{Q_{w\,base}^2 S^2}{C_f^2 B^2 g} \right)^{1/3} \frac{C_{fs}}{RD_g} - \tau_c^* \right) \right]^b + (1-\alpha)\left[\max\left(0, \left(\frac{Q_{w\,peak}^2 S^2}{C_f^2 B^2 g} \right)^{1/3} \frac{C_{fs}}{RD_g} - \tau_c^* \right) \right]^b \tag{30}$$

$$\frac{\bar{Q}_s}{aB\sqrt{RgD_s}D_s(1-F)} = \alpha \left[\max\left(0, \left(\frac{Q_{w\,base}^2 S^2}{C_f^2 B^2 g} \right)^{1/3} \frac{C_{fs}}{RD_s} - \tau_c^* \right) \right]^b + (1-\alpha)\left[\max\left(0, \left(\frac{Q_{w\,peak}^2 S^2}{C_f^2 B^2 g} \right)^{1/3} \frac{C_{fs}}{RD_s} - \tau_c^* \right) \right]^b \tag{31}$$

where the mean gravel and sand loads, $\bar{Q}_g$ and $\bar{Q}_s$, at streamwise coordinate x under conditions with gravel abrasion are predicted using equations (20) and (21), provided that the mean sediment supply rate at the upstream end of the domain $\bar{Q}_0$ and the mean gravel content in the supplied sediment, $\bar{p}_{g0}$, are known. Equations (30) and (31) are easily generalized to account for the arbitrary PDF of water discharge in Figure 1a. This then leads to two relations that allow for solving for two unknowns, provided that the remaining parameters are known.

Analogous to the derivation of the slope-equivalent or channel-forming discharge for unisize sediment in equation (18), we define the channel-forming discharge as that steady water discharge that, given the

gravel supply or the sand supply, provides the same equilibrium channel geometry as the natural long-term hydrograph:

$$\frac{\bar{Q}_g}{aB\sqrt{RgD_g}D_gF} = \left[\max\left(0, \left(\frac{Q_{w\,\mathrm{dom}\,g}^2 S^2}{C_f^2 B^2 g}\right)^{1/3}\frac{C_{fs}}{RD_g} - \tau_c^*\right)\right]^b \tag{32}$$

$$\frac{\bar{Q}_s}{aB\sqrt{RgD_s}D_s(1-F)} = \left[\max\left(0, \left(\frac{Q_{w\,\mathrm{dom}\,s}^2 S^2}{C_f^2 B^2 g}\right)^{1/3}\frac{C_{fs}}{RD_s} - \tau_c^*\right)\right]^b \tag{33}$$

This implies that the steady water discharge that provides the same equilibrium channel slope as the natural long-term hydrograph and transports the gravel load downstream ($Q_{w\,\mathrm{dom}\,g}$) is generally larger than the water discharge that suffices to transport the sand load ($Q_{w\,\mathrm{dom}\,s}$). This difference increases with increasing ratio of gravel size to sand size. Thus, there generally exists no uniquely defined slope-equivalent water discharge.

We also define a total load-related channel-forming discharge, $Q_{w\,\mathrm{dom}}$, which can be solved from

$$\frac{\bar{Q}_g}{aB\sqrt{RgD_g}D_gF} + \frac{\bar{Q}_s}{aB\sqrt{RgD_s}D_s(1-F)} = \left[\max\left(0, \left(\frac{Q_{w\,\mathrm{dom}}^2 S^2}{C_f^2 B^2 g}\right)^{1/3}\frac{C_{fs}}{RD_g} - \tau_c^*\right)\right]^b$$
$$+ \left[\max\left(0, \left(\frac{Q_{w\,\mathrm{dom}}^2 S^2}{C_f^2 B^2 g}\right)^{1/3}\frac{C_{fs}}{RD_s} - \tau_c^*\right)\right]^b \tag{34}$$

This total load-related slope-equivalent discharge, $Q_{w\,\mathrm{dom}}$, is a weighted average of the slope-equivalent water discharges for gravel and sand.

5. Validation of the Analytical Model

We here apply two numerical time-marching models to validate the analytical model for the equilibrium river geometry under variable flow. One time-marching model solves the *Saint-Venant* [1871] equations and the other one the backwater equation [e.g., *Parker*, 2004b]. In the latter model the flow rate varies yet the flow is assumed steady at each time, whereas the first model accounts for the dynamics of flood waves.

The time-marching model runs are made using the one-dimensional numerical research code Elv, which solves for (1) the flow, (2) bed elevation, and (3) surface texture in a decoupled manner. The Saint-Venant equations are solved using an implicit Preismann scheme. Specific settings comprise the time step, $\Delta t = 600\,\mathrm{s}$, and the streamwise length of a grid cell, $\Delta x = 2000\,\mathrm{m}$. The morphodynamic state regarding bed elevation and bed surface texture is updated after each hydrodynamic update. The backwater equation is solved in a space-marching manner, starting from the downstream end and computing the solution in upstream direction (as the flow is subcritical) using a first-order explicit Euler scheme. The streamwise grid size is again $\Delta x = 2000\,\mathrm{m}$, and the flow solver does not require a time step. Bed elevation and bed texture are updated after each time step ($\Delta t = 1\,\mathrm{day}$) using the *Exner* [1920] and *Hirano* [1971] equations.

The streamwise gradients in the gravel and sand loads are computed using a second-order, centered, finite difference stencil. In case of aggradation the grain size distribution of the depositional flux to the substrate is set equal to the one of the active layer [*Hirano*, 1971], yet application of the *Hoey and Ferguson* [1994] formulation for the depositional flux does not change the results. We keep track of changes to the substrate sediment associated with changes in mean bed elevation. The active layer thickness, the vertical size of the grid cells for keeping track of the bed stratification, porosity, and the initial conditions of the time-marching runs (bed elevation, surface, and substrate texture) do not affect the equilibrium channel slope and bed surface texture.

The models are applied to a base case that is characterized by a cycled synthetic hydrograph governed by two peaks and a period of 1 year (Figure 3). That is to say, every year the same synthetic hydrograph is imposed. The simple shape of the hydrograph creates an unnatural shape of the PDF of water discharge yet suffices here. In the base case we impose channel width ($B = 250\,\mathrm{m}$) and solve for channel slope and bed surface texture.
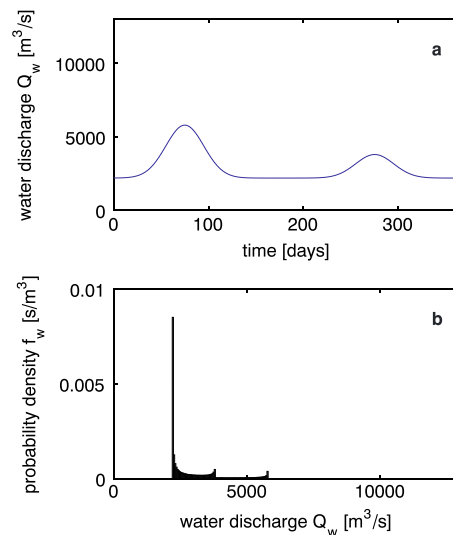
Figure 3. (a) Synthetic hydrograph at the upstream end of the reach and (b) the associated PDF of water discharge.

We run the models for different values of the mean gravel content in the supplied sediment. The domain length is 400 km. The friction coefficient, C_f, equals 0.008, and for simplicity we assume that friction is associated with skin friction only. The mean sediment supply rate equals 0.03 m^3/s. The abrasion coefficient β here equals 0 m^{-1}, and the gravel and sand sizes are 20 mm and 1 mm, respectively.

We apply three load relations: the generalized power law load relation (GR, settings $r = 0.05$, $w_g = w_s = w = 0.4$, and $c = 2.3$) in equation (19), the *Wilcock and Crowe* [2003] load relation (WC), and the *Ashida and Michiue* [1972] load relation (AM). Just as the GR relation, the *Wilcock and Crowe* [2003] load relation does not consist of a threshold for significant transport, whereas the *Ashida and Michiue* [1972] load relation is threshold based.

The outcomes of the analytical model are nearly identical to the results of the two numerical time-marching models (Figure 4). For the time-marching models we consider a position 20 km downstream from the upstream end of the domain, which is sufficiently upstream from the backwater zone. Figure 4 confirms the applicability of the analytical model under normal f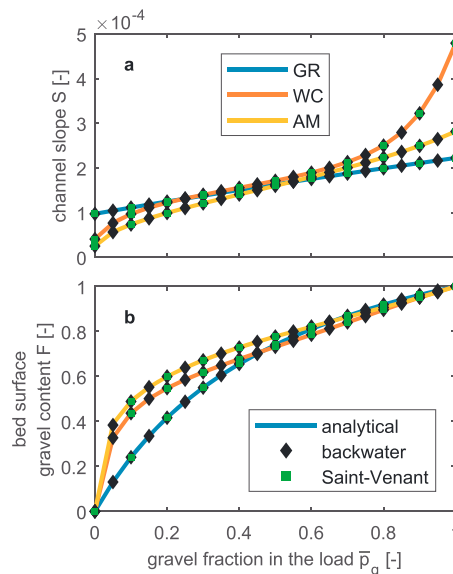low conditions where the effects of the dynamics of flood waves (wave flattening and lengthening) are negligible. If the dynamics of flood waves are not negligible, the statistics of the local hydrograph need to be known from measured data, modeling, or otherwise.

Figure 4. Validation of the analytical model: (a) equilibrium channel slope, S, in the river normal flow zone, and (b) equilibrium bed surface gravel content, F, predicted using the analytical model and two numerical time-marching models as a function of the mean gravel content in the load, $\bar{p}_g$. The data of the time-marching models are associated with a location 20 km downstream from the upstream end of the domain. Predictions are made based on the generalized power law load relation (GR, settings $r = 0.05$, $w_g = w_s = w = 0.4$, and $c = 2.3$) in equation (19), the *Wilcock and Crowe* [2003] load relation (WC), and the *Ashida and Michiue* [1972] load relation (AM).

Figure 4 also shows how both channel slope and bed surface gravel content increase with increasing mean gravel content in the sediment supply, which confirms the analysis by *Blom et al.* [2016].

The PDF of the flow rate needs to cover the statistics of the flow over some years or decades. The analytical model accounts for that long-term variability of the flow rate. The order of flow events or history is here irrelevant since in the considered normal flow zones the equilibrium state is a static one.

The analytical model enables us to rapidly find a solution to the equilibrium river geometry under variable flow (numerical time-marching models take much longer to compute this) and provides insight on the relation among the gravel and sand supply rates, the PDF of water discharge, channel slope, channel width, and bed surface texture. In addition, due to the complexities of
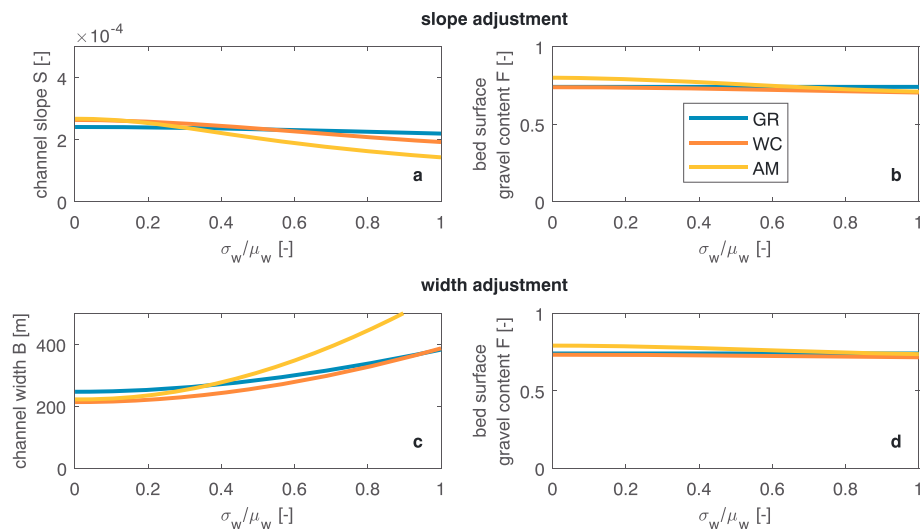
Figure 5. Predicted channel response to a changing boundary condition through (a and b) adjustment of channel slope versus (c and d) adjustment of channel width. The considered boundary condition is the variability of the flow rate, which is expressed by σ_w/μ_w with σ_w denoting the standard deviation of the flow rate and μ_w its mean value. Predicted equilibrium values in the river normal flow zone, for the case of adjustment of channel slope, of channel slope, S (Figure 5a), surface gravel content, F (Figure 5b), and, for the case of adjustment of channel width, channel width, B (Figure 5c), and surface gravel content, F (Figure 5d). Predictions are made using the explicit and implicit analytical models based on the generalized power law load relation (GR, settings $r = 0.05$, $w_g = w_s = w = 0.4$, and $c = 2.3$) in equation (19), the *Wilcock and Crowe* [2003] load relation (WC), and the *Ashida and Michiue* [1972] load relation (AM).

(modeling) bank erosion processes [*Stecca et al.*, 2017], currently available time-marching models may not be capable of simulating channel response through width adjustment.

6. Channel Response Through Slope or Width Adjustment

The importance of the variability of the flow rate or the PDF of water discharge is illustrated by the following example of an engineered river with fixed banks. Let us compare two cases (A and B) that are equal except for the larger standard deviation of the water discharge in Case A. This difference, for a given channel width, results in a smaller equilibrium channel slope in Case A. A larger standard deviation of the water discharge results in a larger channel-forming discharge, and so a smaller channel slope suffices to transport the same amount of sediment downstream.

Rather than response through slope adjustment (through reach-scale aggradation/degradation or changes in channel sinuosity), river response to changes in the boundary conditions may occur through width adjustment [e.g., *Curtis et al.*, 2010; *Dade et al.*, 2011; *Tealdi et al.*, 2011; *Buffington*, 2012]. For reaches where the time scale of slope adjustment is much larger than the time scale of width adjustment [*Howard*, 1980], the explicit solution for the channel slope in equation (26) was rewritten to a solution to the channel width in equation (29), which illustrates that for this type of channel response (i.e., through width adjustment) the larger standard deviation of the water discharge in Case A yields a larger equilibrium channel width. We expect that generally, channel response (to changing boundary conditions) is of a mixed type, so through adjustment of a combination of (1) channel width, (2) channel slope, and (3) surface texture [e.g., *Buffington and Montgomery*, 1999; *Dade et al.*, 2011]. In such a case one will need to add a closure relation to the proposed formulations.

We here assess channel response to changes in the variability of the flow rate applying a lognormal distribution of the flow rate with a mean value of the flow rate, μ_w, equal to 2000 m³/s. Parameters of the base case include $\bar{p}_{g0} = 0.5$, $S = 2.4 \cdot 10^{-4}$, and $B = 250$ m. For an engineered river with fixed banks that responds to changes in the controls through adjusting its slope, Figure 5a confirms that the equilibrium channel slope decreases with increasing variability of the flow rate.

The equilibrium surface texture only mildly responds to changes in the variability of the flow rate (Figure 5b). This result may be surprising as field and flume studies have shown that changes in sediment supply can be

accommodated by small changes in surface texture [*Dietrich et al.*, 1989; *Buffington and Montgomery*, 1999; *Ferguson et al.*, 2015]. Adjustment of surface texture can indeed accommodate changes in sediment supply, yet a change in the characteristic flow rate likely does not affect the surface texture [*Litty and Schlunegger*, 2016; *Blom et al.*, 2016] and, under a constant width, is generally accommodated through channel slope adjustment [*Blom et al.*, 2016, Figure 2].

For a river that responds to changing boundary conditions through adjusting its channel width, Figure 5c confirms that for otherwise equal parameters, the equilibrium channel width increases with increasing variability of the flow rate.

The equilibrium surface texture hardly responds to an increasing variability of the flow rate: the bed surface becomes slightly finer with increasing variability of the flow rate (Figures 5b and 5d). This holds for both types of channel response. In addition, the similarity between Figures 5b and 5d illustrates that remarkably, for the considered case, the type of channel response (through either width or slope adjustment) has almost no effect on the limited adjustment of the surface texture to the changing variability of the flow rate.

7. The Normal Flow Load Distribution and the Hydrograph Boundary Layer

The equilibrium channel slope, width, and surface texture adjust such that they enable the stream to transport the long-term mean sediment supply downstream. In the river normal flow zone the effect of the short-term variation of the sediment supply is not felt. Worded differently, the river normal flow zone is located so far downstream that there is no effect of the short-term variation of the sediment supply on reach-averaged parameters. As such, in a river normal flow zone the local river geometry (channel slope, surface texture, and channel width) is determined by the long-term mean value of the sediment supply and not by its short-term temporal variation.

The resulting equilibrium river geometry determines the distribution of the sediment flux over the period of the cycled hydrograph (i.e., over the range of discharge values). This distribution of the gravel and sand load over the range of water discharge in a river normal flow zone is here termed the normal flow load distribution of gravel and sand.

The fact that the sedigraph (in the field or imposed as a boundary condition in a numerical model) at the upstream end of a reach is generally different from the sedigraph in the river normal flow zone (i.e., the normal flow load distribution) leads to the presence of the "hydrograph boundary layer" (HBL) [e.g., *Parker*, 2004a; *Wong and Parker*, 2006; *Parker et al.*, 2008; *Viparelli et al.*, 2011; *An et al.*, 2017a, 2017b], which is illustrated in Figure 6. This HBL is the adaptation zone over which the distribution of the (gravel and sand) load over the range of the water discharge spatially adjusts toward its normal flow load distribution. An HBL is characterized by downstream migrating fluctuations in bed elevation, slope, and bed surface texture that may dampen with streamwise position [e.g., *Parker et al.*, 2008].

The length of the river normal flow zone is influenced (i.e., reduced) by both the upstream HBL and the downstream backwater zone. Such HBL and backwater effects not only occur at, respectively, the upstream and downstream ends of a reach (Figure 6) but also arise from a spatial change in channel width or friction, a bifurcation, or a tributary. The normal flow zone is the reach that remains when HBL zones and backwater zones are subtracted.

We represent the normal flow load distribution for gravel, sand, and total load using the parameter, v_X (s/m^3):

$$v_X(Q_w) = \frac{Q_X(Q_w)f_w(Q_w)}{\bar{Q}_X} \tag{35}$$

where $X \in \{g, s, t\}$. For $X = g$ the parameter Q_X (m^3/s) indicates the gravel load, for $X = s$ the sand load, and for $X = t$ the total load. The parameter $\bar{Q}_X$ indicates the expected value of the parameter Q_X, which normalizes v_X such that the integral of v_X over water discharge equals unity. As an example, $v_g(Q_w)$ is the probability density of the gravel load transported at a water discharge Q_w.

Given the mean gravel and sand supply, the analytical model allows for predicting the normal flow load distribution for each size fraction. We illustrate this for a simplified Rhine River case, which is a typical example of an engineered river that responds to changes in the controls through slope adjustment. Figure 7 shows the measured water discharge in the Rhine at Lobith in the German-Dutch border area in the period 1901–2013,
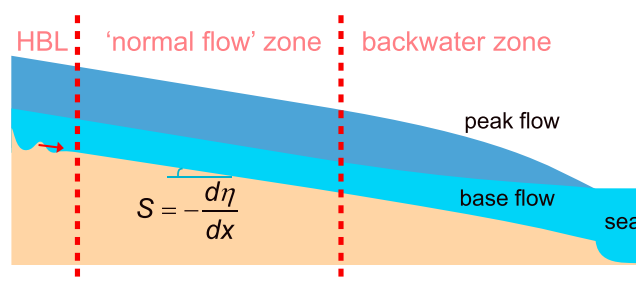
Figure 6. Schematic of variable flow under a constant base level: the hydrograph boundary layer (HBL), the normal flow zone, and the backwater zone.

as well as the associated PDF of the water discharge. Now for illustration purposes, let us assume that normal flow prevails at Lobith. Furthermore, we impose the mean sand load at Lobith equal to 0.56 Mt/a and the mean gravel load to 0.11 Mt/a [*Frings et al.*, 2014, 2015]. We set the channel width, B, equal to 300 m (width over which sediment is transported), the nondimensional friction coefficients, C_f and C_{fs}, to 0.007, the sand size, D_s, to 1 mm, and the gravel size, D_g, to 10 mm.

Table 2 lists values of the equilibrium channel slope and bed surface gravel content at Lobith predicted based on the three load relations applied in section 5. The predicted values of the channel slope are similar. According to *Frings* [2011], the channel slope at Lobith is about $11 \cdot 10^{-5}$ [*Frings*, 2011, Figure 1] and the surface gravel content equals more or less 0.6 [*Frings*, 2011, Figure 6], which implies that the predicted value of the equilibrium channel slope is somewhat smaller than the measured slope. This results in channel bed degradation, which is indeed the case in the German and Dutch Rhine although the reach around Lobith seems to have stabilized over the past few years [*Blom*, 2016]. Despite the model simplifications, the Lobith case illustrates how the analytical model can be applied as a tool for rapid assessment of the equilibrium river geometry and can aid in the assessment of the need for a more detailed study using a time-marching numerical model.

Figure 8 shows the predicted normal flow load distributions for the gravel, sand, and the total load for the three load relations. The results obtained with the threshold-based *Ashida and Michiue* [1972] load relation (Figure 8c) are significantly different from those obtained with the other two relations, which do not account for a threshold for significant transport. A threshold-based load relation results in gravel immobility for small values of the flow rate or the gravel transport being limited to relatively high flow rates. For the generalized load relation (GR) and the *Wilcock and Crowe* [2003] load relation (WC), the distribution of the gravel load, v_g, is closer to the distribution of the water discharge, f_w.
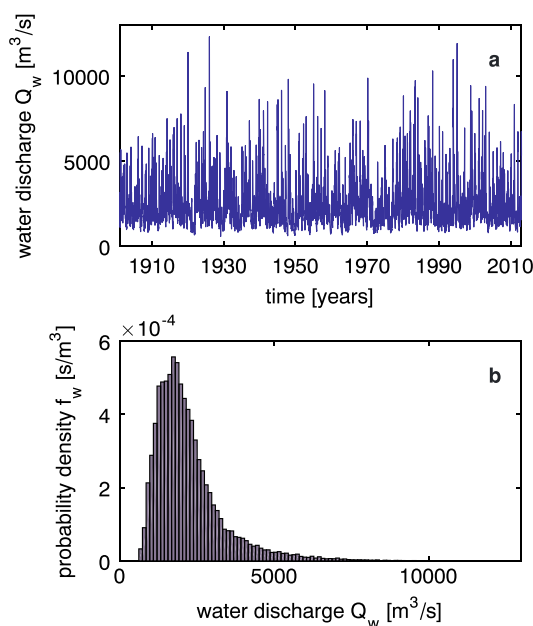

Figure 7. Measured flow rate in the Rhine River at Lobith in the period 1901–2013 (data courtesy: Rijkswaterstaat): (a) the water discharge and (b) the associated probability density function.

Figure 8 confirms the ideas by *Wolman and Miller* [1960] in that extreme flow events, which are largely relevant to flood risk assessment, are of much less importance to the equilibrium river geometry as these peak flow rates do not occur sufficiently frequently to contribute significantly to transporting the supplied sediment load downstream.

8. The Channel-Forming Versus the Effective Discharge

We here compare the slope-equivalent or channel-forming discharges for the gravel and sand load, $Q_{w\,\mathrm{dom}\,g}$ and $Q_{w\,\mathrm{dom}\,s}$, in equations (32) and (33) and the one of the total load $Q_{w\,\mathrm{dom}}$ in equation (34) to the effective discharge first defined by *Wolman and Miller* [1960]. We distinguish between gravel, sand, and total load effective discharges. The gravel-related effective discharge, $Q_{w\,\mathrm{eff}\,g}$, is the water discharge at which the product of the probability density of the water

Table 2. Measured and Predicted Channel Slope S and Bed Surface Gravel Content, F, at Lobith[a]

		Measured	GR	WC	AM
S	$\cdot 10^{-5}$ (−)	11	5.7	5.6	4.8
F	(−)	0.6	0.31	0.47	0.53

[a]Predictions are based on the generalized power law load relation (GR, settings $r = 0.05$, $w_g = w_s = w = 0.4$, and $c = 2.3$) in equation (19), the *Wilcock and Crowe* [2003] load relation (WC), and the *Ashida and Michiue* [1972] load relation (AM), under the assumption of normal flow and the hydrograph shown in Figure 7. Measured data originate from *Frings* [2011].

discharge and the associated gravel load reaches a maximum value, and the sand-related and total load-related effective discharges, $Q_{w\,\text{eff}\,s}$ and $Q_{w\,\text{eff}}$, are defined likewise:

$$Q_{w\,\text{eff}\,g} = \text{mode}(Q_g(Q_w)f_w(Q_w)) \tag{36}$$

$$Q_{w\,\text{eff}\,s} = \text{mode}(Q_s(Q_w)f_w(Q_w)) \tag{37}$$

$$Q_{w\,\text{eff}} = \text{mode}\left((Q_g(Q_w) + Q_s(Q_w))f_w(Q_w)\right) \tag{38}$$

As the current settings of the generalized load relation ($w_i = w$, independent of grain size) do not allow for a coarsening of the load with increasing Shields stress, the normal flow load distributions for gravel, sand, and total load are equal, as well as the channel-forming water discharges for gravel, sand, and the total load. For other settings or other load relations the channel-forming water discharge associated with the gravel load is typically larger than the one associated with the sand load. This also holds for the effective discharges,
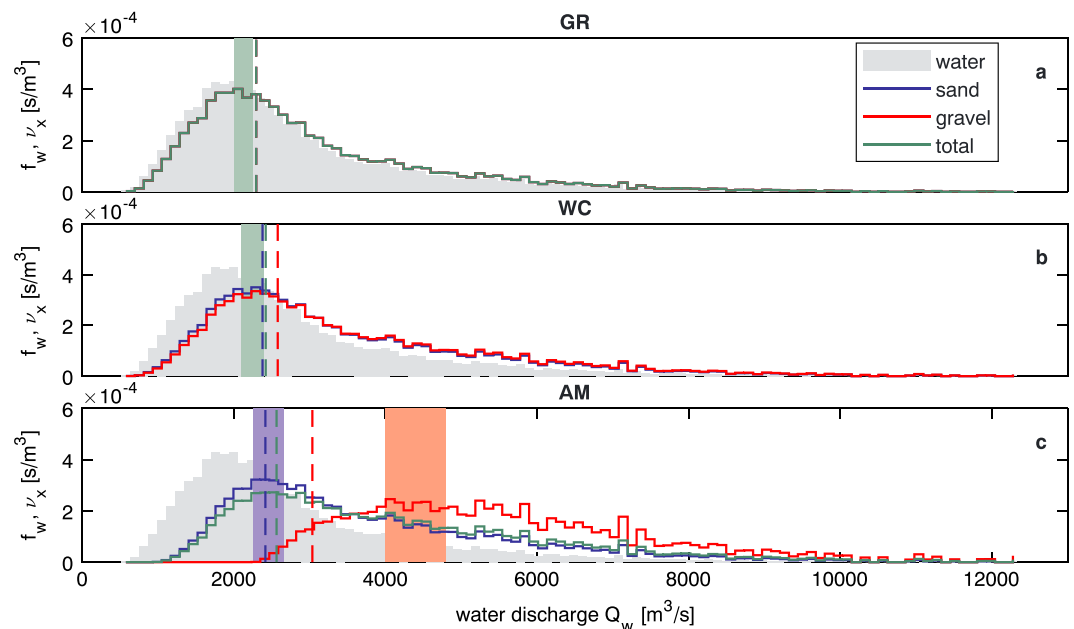

Figure 8. The predicted normal flow load distribution, ν_X, for gravel (in red), sand (in blue), and the total load (in green), which expresses the contribution of the long-term range of water discharge to transporting the gravel, sand, and total load, for the Lobith case shown in Figure 7. Analytical predictions are made based on (a) the generalized power law load relation (GR, settings $r = 0.05$, $w_g = w_s = w = 0.4$, and $c = 2.3$) in equation (19), (b) the *Wilcock and Crowe* [2003] load relation (WC), and (c) the *Ashida and Michiue* [1972] load relation (AM). The dashed vertical lines indicate the channel-forming discharge, and the vertical bars indicate the effective discharge (sand in blue, gravel in red, and total in green). The grey area is the PDF of water discharge, f_w.

which supports findings by *Lenzi et al.* [2006] in that in a mountain stream the bed load-associated effective discharge is larger than the one associated with suspended load.

For the generalized load relation (GR) and the *Wilcock and Crowe* [2003] load relation (WC), the channel-forming discharges are similar to their effective counterparts (Figures 8a and 8b). For threshold-based load relations (such as the *Ashida and Michiue* [1972] load relation, Figure 8c), the discharge values contributing to transporting the gravel load are significantly larger than for load relations without such a threshold (GR and WC). This results in a larger channel-forming discharge (particularly for the gravel load) compared to non-threshold load relations. However, threshold-based relations may overpredict to some extent given that they erroneously predict zero transport at flows below the threshold [e.g., *Barry et al.*, 2004, 2007], which can cover a substantial range of the PDF of the flow rate. For the threshold-based relation (Figure 8c) the gravel-related effective discharge appears to be significantly larger than its channel-forming counterpart.

In addition, for the threshold-based load relation in Figure 8c, the gravel-related channel-forming discharge is associated with a Shields stress ($\tau_g^* = 0.033$) that is only slightly larger than its critical value ($\tau_{cg}^* = 0.027$). This is consistent with findings with respect to the bankfull discharge in gravel-bed rivers [*Parker*, 1978b, 2004b; *Parker et al.*, 2007; *Phillips and Jerolmack*, 2016; *Pfeiffer et al.*, 2017]. The sand-related channel-forming discharge in Figure 8c is associated with a Shields stress ($\tau_s^* = 0.29$) that is significantly larger than its critical value ($\tau_{cs}^* = 0.14$), which is consistent with the findings by *Parker* [1978a, 2004b].

9. Discussion

The definition of *Copeland et al.* [2005] of the dominant or channel-forming discharge is *the single steady discharge that given enough time would produce channel dimensions equivalent to those shaped by the natural long-term hydrograph*. Here we further narrow down the definition of the channel-forming discharge as the steady discharge that, given a certain mean sediment load, provides the same equilibrium channel slope as the natural long-term hydrograph. This slope-equivalent discharge corresponds to the functional-equivalent discharge introduced by *Doyle and Shields* [2008], although they do not explicitly consider the limitation to equilibrium or graded conditions and do not extend their analysis to mixed-sediment conditions. In our analysis we have addressed the relation between the slope-equivalent discharge and the commonly applied effective discharge [e.g., *Wolman and Miller*, 1960], yet we have not addressed the relation with the bankfull discharge. We recommend further research on this topic.

The validity of the proposed formulations is limited to the normal flow zones of a graded or equilibrium alluvial river and does not provide formulations for the zone of the HBL and the backwater zone (Figure 6). The HBL has been studied by *Parker* [2004a], *Wong and Parker* [2006], *Parker et al.* [2008], *Viparelli et al.* [2011], and *An et al.* [2017a, 2017b]. Current research by the second author focuses on a formulation of the equilibrium channel slope in backwater-dominated zones of an alluvial river.

Our analysis is limited to equilibrium river reaches under conditions without subsidence and uplift. Under transient or ungraded conditions [e.g., *Howard*, 1982], in which the river is adjusting to changes in the boundary conditions, river characteristics approach those of the equilibrium or graded river geometry described in this paper. Such temporal adjustment toward the graded river geometry is usually simulated or reproduced using time-marching numerical models. Yet if the change of the boundary conditions happens slowly (i.e., the time scale of change is large compared to the time scale of channel response to the changing boundary conditions), reach characteristics keep pace with the changing boundary conditions. Under such quasi-equilibrium conditions [*Mackin*, 1948; *Chorley and Kennedy*, 1971; *Howard*, 1982] one may apply the formulations proposed in the present paper. *Blom et al.* [2017] consider the case of an abrupt gravel-sand transition, where they apply equilibrium formulations for channel slope and surface texture to quasi-equilibrium conditions.

We have limited our analysis to cases with one or two sediment fractions (gravel and sand), as rivers are often characterized by bimodal distributions of grain size. However, also cases with more than two grain size classes allow for an implicit solution to the equilibrium river geometry.

Simplifications such as the rectangular cross section and the neglect of floodplain processes need to be a point of attention when applying the presented analytical models to a field case. Yet it is precisely these simplifications that allow us to arrive at the explicit and implicit analytical solutions to the equilibrium river geometry. The formulations are specifically meant to provide insight and can be used as a tool for rapid

assessment of the river response to changes in the controls, but application to a field case should always be undertaken with care. Most of the simplifications made in the current analysis may be relaxed by applying a time-marching numerical model to compute the equilibrium river geometry, yet the required computational time may make this impossible.

Concerning the assumption of a rectangular cross section, we expect that a field site with a clear division between main channel and floodplains could be assessed with the analytical model through, for instance, the assumption that the Shields stress does not increase with flow rate once the flow rate exceeds a bankfull value (i.e., under overbank flow conditions). A complication here is the fact that the bankfull flow rate depends on the predicted equilibrium channel slope, surface texture, and channel width. Another strategy could be to include a relation between the flow rate and the cross-sectional area.

Despite the drawbacks associated with the simple form of the power law load relation, we believe that its explicit solutions provide useful insight on how channel slope, width, and surface texture on the long term respond to changes in the boundary conditions. Although the explicit solutions do not account for the fact that the mobility difference between fine and coarse sediment becomes smaller with increasing flow rate, it does account for grain size selectivity (i.e., for the mobility difference between fine and coarse sediment). When applying it to a field case, its constants need to be carefully adjusted to the considered field site and preferably their values need to be validated against data from the field site that were not used in calibrating them. One should apply a more advanced (yet mathematically less convenient) load relation when the power law load relation is insufficiently applicable to the specific field case.

In our time-marching numerical runs we have neglected temporal change of the active layer thickness and bed load layer thickness [*Armanini and Di Silvio*, 1988; *Parker*, 1991]. In reality the depth of reworking of bed sediment during peak flow is larger than during base flow. We recommend further research on this matter.

The current analysis has implications for the schematization of the hydrograph and grain size-specific sedigraphs in long-term numerical runs. The imposed hydrograph should cover the natural long-term hydrograph (i.e., the long-term statistics of the flow rate), yet the tails of the distribution of the flow rate may be less important if one is interested in modeling morphodynamic change in a river normal flow zone.

For field-scale applications of the present formulation, the following field measurements should be preferably available: (1) long-term time series of water discharge or its PDF (at least covering a few years), (2) annual volume of sediment supply or long-term mean sediment supply rate, (3) mean fraction content of gravel in the sediment supply, (4) a representative gravel size, (5) a representative sand size, (6) friction, (7) channel slope, (8) surface fraction content of gravel, and (9) channel width. Field cases for which this data set, especially items 2 and 3, is available are rare. We here underline the importance of acquiring field data on the mean annual gravel and sand flux.

10. Conclusions

We provide analytical formulations for the geometry of an equilibrium alluvial channel under variable flow. The analysis is limited to the normal flow reaches of a river, that is, to reaches outside the hydrograph boundary layer and the backwater zone. The analysis applies to both unisize sediment and sediment mixtures composed of gravel and sand. It accounts for grain size selective transport and particle abrasion.

Application of a power law load relation results in explicit analytical solutions to the relation among the equilibrium channel slope, channel width, and bed surface texture. Application of other load relations (e.g., including a threshold for significant transport, a hiding coefficient, or a load relation that is a conditional function such as the one proposed by *Wilcock and Crowe* [2003]) provides implicit analytical solutions that can be solved iteratively.

The resulting equations aid in the prediction of long-term channel response to changes in the boundary conditions. A river responds to such changes through adjustment of (a) channel slope, (b) channel width, (c) surface texture, or (d) a combination of these types. In engineered rivers where the channel width is fixed, given the sediment supply and PDF of water discharge, there exists one solution to the equilibrium or graded river geometry in a river normal flow zone [e.g., *Parker*, 1990a; *Buffington*, 2012]. In natural streams besides slope also channel planform adjusts to changing conditions through width changes, which implies that there exists a range of equilibrium states for which the channel is able to transport the load supplied from above.

We propose two analytical relations linking: (1) PDF of flow rate, (2 and 3) gravel and sand supply rates, (4) channel width, (5) channel slope, (6) surface texture, and (7 and 8) the representative gravel and sand sizes. The relations can be used to solve for two unknown parameters. In engineered rivers, given the PDF of the flow rate and the sediment supply rates, one can solve for the equilibrium slope and surface texture. In natural streams where the time scale of slope adjustment is much larger than the one of width adjustment, one may impose the channel slope and use the formulations to solve for the equilibrium channel width. In natural streams in which channel response to changing boundary conditions is of a mixed nature (i.e., through adjustment of a combination of slope, width, and surface texture), one may add an empirical relation to the proposed formulations and solve for the combined set of parameters.

The equilibrium surface texture hardly responds to changing variability of the flow rate. In addition, in the considered case the type of channel response to the changing flow rate variability (i.e., through adjustment of either channel slope or channel width) hardly affects how the surface texture adjusts to the changing flow rate variability.

We here define the slope-equivalent or channel-forming discharge as the steady water discharge that provides the same equilibrium channel slope as the natural long-term hydrograph, given the mean sediment supply rate. Application of the power law load relation allows for an explicit analytical solution to the channel-forming discharge in the river normal flow zone. This slope-equivalent discharge is associated with a grain size class: the gravel-related channel-forming discharge is generally larger than the one for sand.

Our definition of the slope-equivalent discharge confirms the ideas by *Wolman and Miller* [1960] in that channel form and so the representative discharge are a function of both the magnitude and frequency of the flow rate. The analysis illustrates that extreme flow events, which naturally are important in flood risk assessment, are less important to the equilibrium river geometry because of their rarity. Worded differently, the tails of the PDF of the flow rate seem to be of limited importance to the equilibrium river geometry in a river normal flow zone. In addition, this implies that, if the effects of climate change are mostly limited to the tails of the PDF of the flow rate, effects of climate change on river geometry may be negligible.

In the equilibrium state the reach-averaged parameters of a river normal flow zone are not affected by the short-term variation of the sediment supply. As such, in a river normal flow zone the local river geometry (channel slope, surface texture, and channel width) is determined by the long-term mean value of the sediment supply and not by its short-term variation.

The analytical model allows for predicting how the gravel and sand load vary over the long-term range of flow rate values in the river normal flow zone, which we term the normal flow load distributions of gravel and sand. The fact that (in the field or the numerically imposed) sedigraphs for gravel and sand at the upstream end of a reach generally differ from their normal flow load distributions leads to the presence of the hydrograph boundary layer.

When applying a threshold-based load relation, we find that the gravel-related channel-forming discharge is only slightly larger than the one associated with its critical Shields number, whereas the difference for the two corresponding values for the sand load is significantly larger. These findings are consistent with earlier findings regarding the bankfull discharge.

The proposed formulations can easily be extended with empirical relations between, for instance, drainage area and channel width or water discharge [e.g., *Hack*, 1957; *Tucker and Bras*, 1998] to find drainage area-based relations for the graded channel slope, width, and surface texture.

The formulations for the equilibrium river geometry provide useful and rapid insight on the state that the river approaches and the long-term consequences of (foreseen) river measures or natural change of the controls [e.g., *De Vriend*, 2015].

The relevance of the statistical equilibrium state of streams seems to be broader than is generally anticipated. It has often been argued that the river's equilibrium state is irrelevant as it may never arrive at that state due to continuously changing boundary conditions and uplift or subsidence. Yet if the controls change so slowly that the stream can keep pace with them, the stream continuously finds itself in a state of quasi-equilibrium,

in which the proposed formulations can be applied. This is illustrated by *Blom et al.* [2017] for the case of an abrupt gravel-sand transition.

Appendix A: Generalized Load Relation for Unisize Sediment

We summarize the wide range of existing power law load relations into the following generalized relation:

$$W^* = c \left(\frac{D}{D_{\text{ref}}} \right)^r \tau^{*w} \tag{A1}$$

where c (−), w (−), and r (−) are constants ($w > r$ for a decreasing sediment load with increasing grain size). The nondimensional sediment transport rate, W^* (−), the nondimensional Einstein transport number, q^* (−), and the grain-related Shields stress or Shields stress associated with skin friction, τ^* (−), are defined as [e.g., *Parker*, 2004b]

$$W^* = \frac{q^*}{\tau^{*3/2}}, \quad q^* = \frac{Q}{B\sqrt{RgD}D}, \quad \tau^* = \frac{\tau_{bs}}{\rho g R D} \tag{A2}$$

where R (−) denotes the submerged sediment density ($R = (\rho_s - \rho)/\rho$ in which ρ_s (kg/m^3) and ρ (kg/m^3) are the sediment and water density, respectively) and g (m/s^2) is the acceleration due to gravity. The grain-related shear stress, τ_{bs} (N/m^2), is defined as $\tau_{bs} = \rho C_{fs} U^2$, where C_{fs} (−) denotes the nondimensional skin friction coefficient and U (m/s) is the depth-averaged flow velocity.

Combining equations (A1) and (A2), we find the following relation for the sediment transport rate per unit width, q (m^2/s) ($Q = qB$):

$$q = \left(\frac{D}{D_{\text{ref}}} \right)^r \frac{G}{D^w} U^{2w+3}, \quad G = \frac{c\,C_{fs}^{w+\frac{3}{2}}}{(Rg)^{w+1}} \tag{A3}$$

Equation (A3) is rearranged into the relation proposed by *Engelund and Hansen* [1967] through setting $w = 1$, $r = 0$, and $c = 0.05 C_f^{3/2}/C_{fs}^{5/2}$:

$$q_{\text{EH}} = \frac{G_{\text{EH}}}{D} U^5, \quad G_{\text{EH}} = \frac{0.05 C_f^{3/2}}{(Rg)^2} \tag{A4}$$

It is important to note that the friction coefficient, C_f, in the *Engelund and Hansen* [1967] load relation contains form drag.

Appendix B: Generalized Load Relation for Mixed Sediment

For mixed sediment we propose the following generalized power law load relation:

$$W_i^* = c \left(\frac{D_i}{D_{\text{ref}}} \right)^r \tau_i^{*w_i} \tag{B1}$$

where w_i (−) is a constant generally slightly increasing with grain size D_i [e.g., *Kuhnle*, 1992]. The nondimensional sediment transport rate of size fraction i, W_i^* (−), the nondimensional Einstein transport number of size fraction i, q_i^* (−), and the grain-related Shields stress associated with size fraction i, τ_i^* (−), are defined as [e.g., *Parker*, 2004b]

$$W_i^* = \frac{q_i^*}{\tau_i^{*3/2}}, \quad q_i^* = \frac{Q_i}{B\sqrt{RgD_i}D_i F_i}, \quad \tau_i^* = \frac{\tau_{bs}}{\rho g R D_i} \tag{B2}$$

where F_i (−) denotes the volume fraction content of size fraction i at the bed surface and D_i (m) is the representative grain size of size fraction i.

Equations (B1) and (B2) lead to the following formulation for the mixed-sediment transport rate per unit width, q_i (m^2/s):

$$q_i = F_i \left(\frac{D_i}{D_{\text{ref}}} \right)^r \frac{G_i}{D_i^{w_i}} U^{2w_i+3} \tag{B3}$$
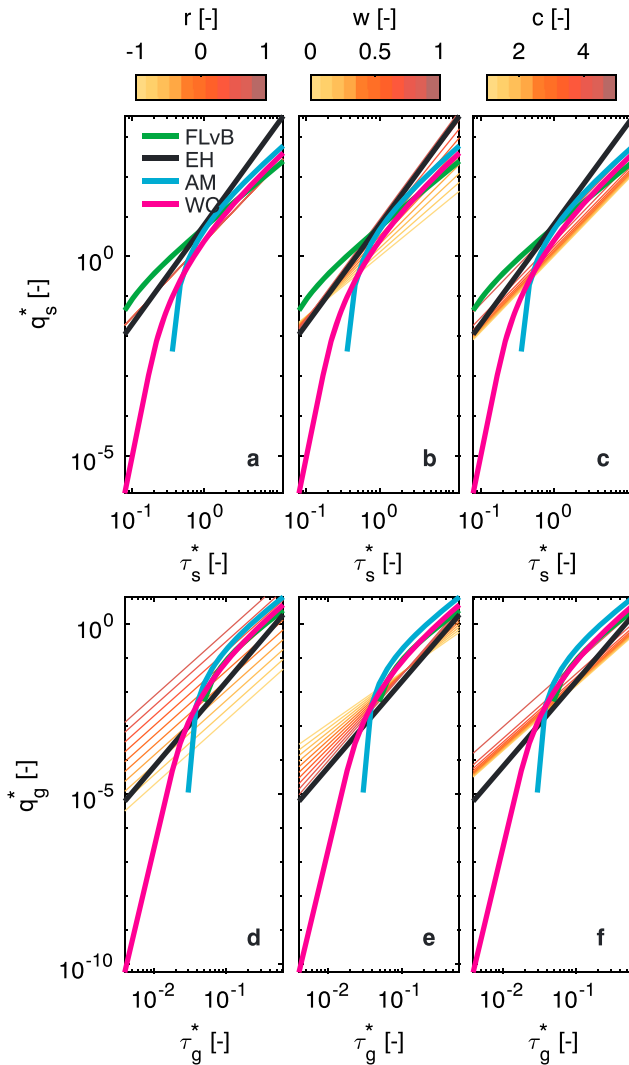
Figure B1. Comparison of the generalized load relation in equation (B1) or (B3) to other load relations for a gravel bedded river with a bed surface consisting of 90% gravel. (a–c) The predicted nondimensional sand load (sand size $D_s = 1$ mm) and (d–f) the gravel load (gravel size $D_g = 10$ mm), for a range of values for r, w ($w_g = w_s = w$), and c. In the base case $r = 0.05$, $w = 0.4$, and $c = 2.3$. Besides the generalized load relation, predictions are made using the *Engelund and Hansen* [1967] (EH), *Fernandez-Luque and Van Beek* [1976] (FLvB), *Ashida and Michiue* [1972] (AM), and *Wilcock and Crowe* [2003] (WC) load relations.

where the constant G_i is defined as

$$G_i = \frac{cC_{fs}^{w_i + \frac{3}{2}}}{(Rg)^{w_i + 1}} \tag{B4}$$

Equation (B3) is cast into the fractional form of the *Engelund and Hansen* [1967] relation by setting $w_i = 1$, $r = 0$, and $c = 0.05C_f^{3/2}/C_{fs}^{5/2}$:

$$q_{i\,EH} = F_i \frac{G_{EH}}{D_i} U^5 \tag{B5}$$

where G_{EH} is defined in equation (A4b). The fractional form of the transport relation by *Engelund and Hansen* [1967] in equation (B5) was proposed nor validated by the original authors yet was applied by *Van der Scheer et al.* [2002] and *Blom et al.* [2016].

In Figure B1 we compare the nondimensional gravel and sand load predicted using the generalized load relation to data predicted using the load relations by *Engelund and Hansen* [1967] (EH), *Fernandez-Luque and Van Beek* [1976] (FLvB), *Ashida and Michiue* [1972] (AM), and *Wilcock and Crowe* [2003] (WC). It shows how the power law load relation covers the general trends fairly well. Figure B1 also indicates the range of reasonable values for r, w_i, and c.

References

An, C., Y. Cui, X. Fu, and G. Parker (2017a), Gravel-bed river evolution in earthquake-prone regions subject to cycled hydrographs and repeated sediment pulses, *Earth Surf. Processes Landforms*, doi:10.1002/esp.4195.

An, C., X. Fu, G. Wang, and G. Parker (2017b), Effect of grain sorting on gravel bed river evolution subject to cycled hydrographs: Bed load sheets and breakdown of the hydrograph boundary layer, *J. Geophys. Res. Earth Surf.*, *122*, 1513–1533, doi:10.1002/2016JF003994.

Ackers, P., and F. G. Charlton (1970), Meander geometry arising from varying flows, *J. Hydrol.*, *11*(3), 230–252, doi:10.1016/0022-1694(70)90064-8.

Ahnert, F. (1994), Equilibrium, scale and inheritance in geomorphology, *Geomorphology*, *11*(2), 125–140, doi:10.1016/0169-555X(94)90077-9.

Andrews, E. D. (1980), Effective and bankfull discharges of streams in the Yampa River basin, Colorado and Wyoming, *J. Hydrol.*, *46*(3-4), 311–330, doi:10.1016/0022-1694(80)90084-0.

Armanini, A., and G. Di Silvio (1988), A one-dimensional model for the transport of a sediment mixture in non-equilibrium conditions, *J. Hydraul. Res.*, *26*(3), 275–292, doi:10.1080/00221688809499212.

Ashida, K., and M. Michiue (1972), Study on hydraulic resistance and bed-load transport rate in alluvial streams, *J. Soc. Civ. Eng. Trans.*, *206*, 59–69, doi:10.2208/jscej1969.1972.206_59.

Barry, J. J., J. M. Buffington, and J. G. King (2004), A general power equation for predicting bed load transport rates in gravel bed rivers, *Water Resour. Res.*, *40*, W10401, doi:10.1029/2004WR003190.

Barry, J. J., J. M. Buffington, and J. G. King (2007), Correction to "A general power equation for predicting bed load transport rates in gravel bed rivers", *Water Resour. Res.*, *43*, W08702, doi:10.1029/2007WR006103.

Benson, M. A., and D. M. Thomas (1966), A definition of dominant discharge, *Int. Assoc. Sci. Hydrol. Bull.*, *11*(2), 76–80, doi:10.1080/02626666609493460.

Biedenharn, D. S., C. C. Watson, and C. R. Thorne (2008), Fundamentals of fluvial geomorphology, in *Sedimentation Engineering: Processes, Measurements, Modeling, and Practice*, edited by M. H. Garcia, pp. 355–386, Am. Soc. Civil Eng., Reston, Va., doi:10.1061/9780784408148.ch06.

Blom, A. (2008), Different approaches to handling vertical and streamwise sorting in modeling river morphodynamics, *Water Resour. Res.*, *44*, W03415, doi:10.1029/2006WR005474.

Blom, A. (2016), Bed Degradation in the Rhine River, WaterViewer. Delft Univ. of Technol. [Available at http://waterviewer.tudelft.nl/#/bed-degradation-in-the-rhine-river-1479821439344___47.]

Blom, A., E. Viparelli, and V. Chavarrías (2016), The graded alluvial river: Profile concavity and downstream fining, *Geophys. Res. Lett.*, *43*, 1–9, doi:10.1002/2016GL068898.

Blom, A., V. Chavarrías, R. I. Ferguson, and E. Viparelli (2017), Advance, retreat, and halt of abrupt gravel-sand transitions in alluvial rivers, *Geophys. Res. Lett.*, *44*, doi:10.1002/2017GL074231.

Bolla Pittaluga, M., R. Luchi, and G. Seminara (2014), On the equilibrium profile of river beds, *J. Geophys. Res. Earth Surface*, *119*, 317–332, doi:10.1002/2013JF002806.

Bray, D. (1975), Representative discharges for gravel-bed rivers in Alberta, Canada, *J. Hydrol.*, *27*(1-2), 143–153, doi:10.1016/0022-1694(75)90103-1.

Buffington, J. M. (2012), Changes in channel morphology over human time scales, in *Gravel-Bed Rivers: Processes, Tools, Environments*, edited by M. Church, P. M. Biron, and A. G. Roy, pp. 433–463, John Wiley, Ltd., Chichester, U. K., doi:10.1002/9781119952497.ch32.

Buffington, J. M., and D. R. Montgomery (1999), Effects of sediment supply on surface textures of gravel-bed rivers, *Water Resour. Res.*, *35*(11), 3523–3530, doi:10.1029/1999WR900232.

Carling, P. (1988), The concept of dominant discharge applied to two gravel-bed streams in relation to channel stability thresholds, *Earth Surf. Processes Landforms*, *13*(4), 355–367, doi:10.1002/esp.3290130407.

Chorley, R. J., and B. A. Kennedy (1971), *Physical Geography: A Systems Approach*, 370 pp., Prentice Hall, London, doi:10.1002/qj.49709841818.

Church, M. (2006), Bed material transport and the morphology of alluvial river channels, *Annu. Rev. Earth Planet. Sci.*, *34*(1), 325–354, doi:10.1146/annurev.earth.33.092203.122721.

Copeland, R., P. Soar, and C. Thorne (2005), Channel-forming discharge and hydraulic geometry width predictors in meandering sand-bed rivers, in *Proceedings of the World Water and Environmental Resources Congress: Impacts of Global Change*, pp. 1–12, ASCE, Reston, Va., doi:10.1061/40792(173)568.

Curtis, K. E., C. E. Renshaw, F. J. Magilligan, and W. B. Dade (2010), Temporal and spatial scales of geomorphic adjustments to reduced competency following flow regulation in bedload-dominated systems, *Geomorphology*, *118*(1–2), 105–117, doi:10.1016/j.geomorph.2009.12.012.

Dade, W. B., C. E. Renshaw, and F. J. Magilligan (2011), Sediment transport constraints on river response to regulation, *Geomorphology*, *126*(1–2), 245–251, doi:10.1016/j.geomorph.2010.11.007.

De Vriend, H. J. (2015), The long-term response of rivers to engineering works and climate change, *Proc. Inst. Civil Eng.*, *168*(3), 139–145, doi:10.1680/cien.14.00068.

De Vries, M. (1971), Aspecten van zandtransport in open waterlopen, *Tech. Rep.*, p. 71, Afd. der Weg- en Waterbouwkunde, Technische Hogeschool Delft, Delft, Netherlands.

De Vries, M. (1974), Sedimenttransport, Lecture Notes F10, p. 65, Delft Univ. of Technol., Delft, Netherlands.

De Vries, M. (1993), *Use of Models for River Problems*, p. 85, UNESCO, Paris.

Dietrich, W. E., J. W. Kirchner, H. Ikeda, and F. Iseya (1989), Sediment supply and the development of the coarse surface layer in gravel-bedded rivers, *Nature*, *340*, 215–217, doi:10.1038/340215a0.

Doyle, M. W., and C. A. Shields (2008), An alternative measure of discharge effectiveness, *Earth Surf. Processes Landforms*, *33*(2), 308–316, doi:10.1002/esp.1543.

Doyle, M. W., D. Shields, K. F. Boyd, P. B. Skidmore, and D. Dominick (2007), Channel-forming discharge selection in river restoration design, *J. Hydraul. Eng.*, *133*(7), 831–837, doi:10.1061/(ASCE)0733-9429(2007)133:7(831).

Einstein, H. A. (1950), The bed-load function for sediment transportation in open channel flows, *Tech. Bull. 1026*, p. 71, U.S. Dep. of Agric., Washington, D. C.

Emmett, W. W., and M. G. Wolman (2001), Effective discharge and gravel-bed rivers, *Earth Surf. Processes Landforms*, *26*(13), 1369–1380, doi:10.1002/esp.303.

Engelund, F., and E. Hansen (1967), Monograph on sediment transport in alluvial streams, *Tech. Rep.*, p. 63, Tech. Univ. of Denmark, Copenhagen, Denmark.

Exner, F. M. (1920), Zur Physik der Dünen, *Akad. Wiss. Wien Math. Naturwiss*, *129*(2a), 929–952.

Ferguson, R. I. (2003), Emergence of abrupt gravel to sand transitions along rivers through sorting processes, *Geology*, *31*(2), 159–162, doi:10.1130/0091-7613(2003)031<0159:EOAGTS>2.0.CO;2.

Ferguson, R. I., M. Church, C. D. Rennie, and J. G. Venditti (2015), Reconstructing a sediment pulse: Modeling the effect of placer mining on Fraser River, Canada, *J. Geophys. Res. Earth Surf.*, *120*, 1436–1454, doi:10.1002/2015JF003491.

Fernandez-Luque, R., and R. Van Beek (1976), Erosion and transport of bed-load sediment, *J. Hydraul. Res.*, *14*(2), 127–144, doi:10.1080/00221687609499677.

Ferrer-Boix, C., and M. A. Hassan (2015), Channel adjustments to a succession of water pulses in gravel bed rivers, *Water Resour. Res.*, *51*, 8773–8790, doi:10.1002/2015WR017664.

Fleischmann, A. S., R. C. D. Paiva, W. Collischonn, M. V. Sorribas, and P. R. M. Pontes (2016), On river-floodplain interaction and hydrograph skewness, *Water Resour. Res.*, *52*, 7615–7630, doi:10.1002/2016WR019233.

Frings, R. M. (2011), Sedimentary characteristics of the gravel-sand transition in the River Rhine, *J. Sediment. Res.*, *81*(1), 52–63, doi:10.2110/jsr.2011.2.

Frings, R. M., R. Döring, C. Beckhausen, H. Schüttrumpf, and S. Vollmer (2014), Fluvial sediment budget of a modern, restrained river: The lower reach of the Rhine in Germany, *Catena*, *122*, 91–102, doi:10.1016/j.catena.2014.06.007.

Frings, R., K. Banhold, and I. Evers (2015), Sedimentbilanz des Oberen Rheindeltas für den Zeitraum 1991–2010, *Tech. Rep. 2015.019*, p. 43, Institut für Wasserbau und Wasserwirtschaft, RWTH Aachen, Germany.

Gasparini, N. M., G. E. Tucker, and R. L. Bras (2004), Network-scale dynamics of grain-size sorting: Implications for downstream fining, stream-profile concavity, and drainage basin morphology, *Earth Surf. Processes Landforms*, *29*(4), 401–421, doi:10.1002/esp.1031.

Gilbert, G. K. (1877), *Report on the Geology of the Henry Mountains*, p. 160, U.S. Govt. Print. Off., Washington, D. C.

Gomez, B., S. E. Coleman, V. W. K. Sy, D. H. Peacock, and M. Kent (2007), Channel change, bankfull and effective discharges on a vertically accreting, meandering, gravel-bed river, *Earth Surf. Processes Landforms*, *32*(5), 770–785, doi:10.1002/esp.1424.

Goodwin, P. (2004), Analytical solutions for estimating effective discharge, *J. Hydraul. Eng.*, *130*(8), 729–738, doi:10.1061/(ASCE)0733-9429(2004)130:8(729).

Hack, J. (1957), *Studies of Longitudinal Stream Profiles in Virginia and Maryland*, p. 59, U.S. Geol. Surv. Prof. Pap. 294-B, U.S. Govt. Print. Off., Washington, D. C.

Hey, R. D. (1996), Channel response and channel forming discharge, *Final Rep. R&D 6871-EN-01*, Univ. of East Anglia, Norwich, U. K.

Hirano, M. (1971), River bed degradation with armoring, *Trans. Japan Soc. Civ. Eng*, *3*(2), 194–195.

Hoey, T. B., and R. Ferguson (1994), Numerical simulation of downstream fining by selective transport in gravel bed rivers: Model development and illustration, *Water Resour. Res.*, *30*(7), 2251–2260, doi:10.1029/94WR00556.

Houssais, M., C. P. Ortiz, D. J. Durian, and D. J. Jerolmack (2015), Onset of sediment transport is a continuous transition driven by fluid shear and granular creep, *Nat. Commun.*, *6*(6527), doi:10.1038/ncomms7527.

Howard, A. D. (1980), Thresholds in river regimes, in *Thresholds in Geomorphology*, edited by D. R. Coates and J. D. Vitek, pp. 227–258, Allen and Unwin, Boston.

Howard, A. D. (1982), Equilibrium and time scales in geomorphology: Application to sand-bed alluvial streams, *Earth Surf. Processes Landforms*, *7*(4), 303–325, doi:10.1002/esp.3290070403.

Jansen, P. Ph., L. van Bendegom, J. van den Berg, M. de Vries, and A. Zanen (1979), *Principles of River Engineering: The Non-Tidal Alluvial River*, p. 509, Pitman London, San Francisco, London.

Klonsky, L., and R. M. Vogel (2011), Effective measures of "effective" discharge, *J. Geol.*, *119*(1), 1–14, doi:10.1086/657258.

Kuhnle, R. A. (1992), Fractional transport rates of bedload on Goodwin Creek, in *Dynamics of Gravel-Bed Rivers*, edited by P. Billi et al., pp. 141–155, John Wiley, Chichester.

Kuhnle, R. A., and J. C. Willis (1992), Mean size distribution of bed load on Goodwin Creek, *J. Hydraul. Eng.*, *118*(10), 1443–1446, doi:10.1061/(ASCE)0733-9429(1992)118:10(1443).

Lacey, G. (1930), Stable channels in alluvium, *Min. Proc. Inst. Civ. Eng.*, *229*, 259–292, doi:10.1680/imotp.1930.15592.

Lane, E. W. (1955), The importance of fluvial morphology in hydraulic engineering, *Proc. Am. Soc. Civ. Eng.*, *81*(754), 1–17.

Lauer, J. W., and G. Parker (2008), Modeling framework for sediment deposition, storage, and evacuation in the floodplain of a meandering river: Theory, *Water Resour. Res.*, *44*, W04425, doi:10.1029/2006WR005528.

Lauer, J. W., E. Viparelli, and H. Piégay (2016), Morphodynamics and sediment tracers in 1-D (MAST-1D): 1-D sediment transport that includes exchange with an off-channel sediment reservoir, *Adv. Water Resour.*, *93*, 135–149, doi:10.1016/j.advwatres.2016.01.012.

Lenzi, M. A., L. Mao, and F. Comiti (2006), Effective discharge for sediment transport in a mountain river: Computational approaches and geomorphic effectiveness, *J. Hydrol.*, *326*(1–4), 257–276, doi:10.1016/j.jhydrol.2005.10.031.

Leopold, L. B., and T. Maddock (1953), *The Hydraulic Geometry of Stream Channels and Some Physiographic Implications*, Prof. Paper 252, p. 64, U.S. Dep. of the Inter., Geol. Surv., Washington, D. C.

Li, C., M. J. Czapiga, E. C. Eke, E. Viparelli, and G. Parker (2015), Variable shields number model for river bankfull geometry: Bankfull shear velocity is viscosity-dependent but grain size-independent, *J. Hydraul. Res.*, *53*(1), 36–48, doi:10.1080/00221686.2014.939113.

Litty, C., and F. Schlunegger (2016), Controls on pebbles' size and shape in streams of the Swiss Alps, *J. Geol.*, *125*(1), 101–112, doi:10.1086/689183.

Mackin, J. H. (1948), Concept of the graded river, *Geol. Soc. Am. Bull.*, *59*(5), 463–512, doi:10.1130/0016-7606(1948)59[463:COTGR]2.0.CO;2.

Meyer-Peter, E., and R. Müller (1948), Formulas for bed-load transport, in *Proceedings of the 2nd Meeting of International Association for Hydraulic Research*, pp. 39–64, IAHR, Stockholm, Sweden.

Mosselman, E. (2009), Bank protection and river training along the braided Brahmaputra-Jamuna River, Bangladesh, in *Braided Rivers: Process, Deposits, Ecology and Management*, edited by G. H. Sambrook Smith et al., pp. 277–287, Blackwell, Oxford, U. K., doi:10.1002/9781444304374.ch13.

Nash, D. B. (1994), Effective sediment-transporting discharge from magnitude-frequency analysis, *J. Geol.*, *102*(1), 79–95.

NEDECO (1959), *River Studies and Recommendations of Niger and Benue*, p. 1000, North-Holland, Amsterdam.

Paola, C. (2001), Modelling stream braiding over a range of scales, in *Gravel-Bed Rivers V*, edited by M. P. Mosley, pp. 11–46, N. Z. Hydrol. Soc., Wellington, New Zealand.

Parker, G. (1978a), Self-formed straight rivers with equilibrium banks and mobile bed: Part 1. The sand-silt river, *J. Fluid Mech.*, *89*(1), 109–125, doi:10.1017/S0022112078002499.

Parker, G. (1978b), Self-formed straight rivers with equilibrium banks and mobile bed: Part 2. The gravel river, *J. Fluid Mech.*, *89*(1), 127–146, doi:10.1017/S0022112078002505.

Parker, G., and P. C. Klingeman (1982), On why gravel bed streams are paved, *Water Resour. Res.*, *18*(5), 1409–1423, doi:10.1029/WR018i005p01409.

Parker, G., S. Dhamotharan, and H. Stefan (1982b), Model experiments on mobile, paved gravel bed streams, *Water Resour. Res.*, *18*(5), 1395–1408, doi:10.1029/WR018i005p01395.

Parker, G. (1990a), Surface-based bedload transport relation for gravel rivers, *J. Hydraul. Res.*, *28*(4), 417–436, doi:10.1080/00221689009499058.

Parker, G. (1990b), The "Acronym" series of Pascal programs for computing bed load transport in gravel rivers, in *External Memorandum M-220*, p. 124, Univ. of Minnesota, St. Anthony Falls Hydraulic Lab., Minn.

Parker, G. (1991), Selective sorting and abrasion of river gravel. I: Theory, *J. Hydraul. Eng.*, *117*(2), 131–147, doi:10.1061/(ASCE)0733-9429(1991)117:2(131).

Parker, G. (2004a), Response of the gravel bed of a mountain river to a hydrograph, in *Proceedings of the International Conference on Slopeland Disaster Mitigation, Taipei Taiwan*, p. 11, St. Anthony Falls Lab., Univ. of Minn.

Parker, G. (2004b), 1D Sediment Transport Morphodynamics With Applications to Rivers and Turbidity Currents, E-Book. [Available at: http://hydrolab.illinois.edu/people/parkerg/morphodynamics_e-book.htm.]

Parker, G., C. Paola, and S. Leclair (2000), Probabilistic Exner sediment continuity equation for mixtures with no active layer, *J. Hydraul. Eng.*, *126*(11), 818–826, doi:10.1061/(ASCE)0733-9429(2000)126:11(818).

Parker, G., P. R. Wilcock, C. Paola, W. E. Dietrich, and J. Pitlick (2007), Physical basis for quasi-universal relations describing bankfull hydraulic geometry of single-thread gravel bed rivers, *J. Geophys. Res.*, *112*, F04005, doi:10.1029/2006JF000549.

Parker, G., M. A. Hassan, and P. Wilcock (2008), Adjustment of the bed surface size distribution of gravel-bed rivers in response to cycled hydrographs, in *Gravel-Bed Rivers VI: From Process Understanding to River Restoration*, vol. 11, edited by H. Habersack, H. Piégay, and M. Rinaldi, pp. 241–285, Elsevier, New York, doi:10.1016/S0928-2025(07)11127-5.

Pfeiffer, A. M., N. J. Finnegan, and J. K. Willenbring (2017), Sediment supply controls equilibrium channel geometry in gravel rivers, *Proc. Natl. Acad. Sci.*, *114*(13), 3346–3351, doi:10.1073/pnas.1612907114.

Phillips, B. C., and A. J. Sutherland (1989), Spatial lag effects in bed load sediment transport, *J. Hydraul. Res.*, *27*(1), 115–133, doi:10.1080/00221688909499247.

Phillips, C. B., and D. J. Jerolmack (2016), Self-organization of river channels as a critical filter on climate signals, *Science*, *352*(6286), 694–697, doi:10.1126/science.aad3348.

Pickup, G., and W. A. Rieger (1979), A conceptual model of the relationship between channel characteristics and discharge, *Earth Surf. Processes Landforms*, *4*(1), 37–42, doi:10.1002/esp.3290040104.

Pickup, G., and R. F. Warner (1976), Effects of hydrologic regime on magnitude and frequency of dominant discharge, *J. Hydrol.*, *29*(1-2), 51–75, doi:10.1016/0022-1694(76)90005-6.

Prins, A. (1969), Dominant discharge, *Tech. Rep. S 78-III*, p. 134, Waterloopkundig Laboratorium Delft, Netherlands.

Prins, A., and M. de Vries (1971), On dominant discharge concepts for rivers, in *Proceedings of the 14th IAHR Congress*, p. 22, IAHR, Paris, France.

Ribberink, J. S. (1987), Mathematical modelling of one-dimensional morphological changes in rivers with non-uniform sediment, *Rep. No. 87-2* PhD thesis, Delft Univ. of Technol., Netherlands.

Saint-Venant, A. J. C. B. (1871), Théorie du mouvement non permanent des eaux, avec application aux crues des rivières et à l'introduction des marées dans leur lit, *Comptes Rendus des séances de l'Académie des Sciences*, *73*, 237–240.

Stecca, G., A. Siviglia, and A. Blom (2014), Mathematical analysis of the Saint-Venant-Hirano model for mixed-sediment morphodynamics, *Water Resour. Res.*, *50*(10), 7563–7589, doi:10.1002/2014WR015251.

Stecca, G., A. Siviglia, and A. Blom (2016), An accurate numerical solution to the Saint-Venant-Hirano model for mixed-sediment morphodynamics in rivers, *Adv. Water Resour.*, *93*(Part A), Part A, 39–61, doi:10.1016/j.advwatres.2015.05.022.

Stecca, G., R. Measures, and D. M. Hicks (2017), A framework for the analysis of noncohesive bank erosion algorithms in morphodynamic modeling, *Water Resources Research*, *53*, 6663–6686, doi:10.1002/2017WR020756.

Surian, N., L. Mao, M. Giacomin, and L. Ziliani (2009), Morphological effects of different channel-forming discharges in a gravel-bed river, *Earth Surf. Processes Landforms*, *34*(8), 1093–1107, doi:10.1002/esp.1798.

Syvitski, J. P., M. D. Morehead, D. B. Bahr, and T. Mulder (2000), Estimating fluvial sediment transport: The rating parameters, *Water Resour. Res.*, *36*(9), 2747–2760, doi:10.1029/2000WR900133.

Tal, M., and C. Paola (2010), Effects of vegetation on channel morphodynamics: Results and insights from laboratory experiments, *Earth Surf. Processes Landforms*, *35*(9), 1014–1028, doi:10.1002/esp.1908.

Tealdi, S., C. Camporeale, and L. Ridolfi (2011), Long-term morphological river response to hydrological changes, *Adv. Water Resour.*, *34*(12), 1643–1655, doi:10.1016/j.advwatres.2011.08.011.

Tucker, G. E., and R. L. Bras (1998), Hillslope processes, drainage density, and landscape morphology, *Water Resour. Res.*, *34*(10), 2751–2764, doi:10.1029/98WR01474.

Van Bendegom, L. (1967), Algemene waterbouwkunde. Deel I: De natuur, *Tech. Rep.*, Afd. der Weg- en Waterbouwkunde, Technische Hogeschool Delft, Netherlands.

Van der Scheer, P., J. S. Ribberink, and A. Blom (2002), Transport formulas for graded sediment: Behaviour of transport formulas and verification with data, *Tech. Rep. 2002R-002*, p 124. Univ. of Twente, Netherlands.

Vargas-Luna, A. (2016), Role of vegetation on river bank accretion, PhD thesis, p. 241, Delft Univ. of Technol., Netherlands, doi:10.4233/uuid:286c36e8-3cac-403c-9d0a-72a5232c5093.

Viparelli, E., D. Gaeuman, P. Wilcock, and G. Parker (2011), A model to predict the evolution of a gravel bed river under an imposed cyclic hydrograph and its application to the Trinity River, *Water Resour. Res.*, *47*, W02533, doi:10.1029/2010WR009164.

Viparelli, E., J. W. Lauer, P. Belmont, and G. Parker (2013), A numerical model to develop long-term sediment budgets using isotopic sediment fingerprints, *Comput. Geosci.*, *53*, 114–122, doi:10.1016/j.cageo.2011.10.003.

Viparelli, E., R. R. H. Moreira, and A. Blom (2017), Modelling stratigraphy-based gravel-bed river morphodynamics, in *Gravel Bed Rivers: Process and Disasters*, edited by D. Tsutsumi and J. B. Laronne, pp. 609–637, John Wiley, Chichester, U. K., doi:10.1002/9781118971437.ch23.

Vogel, R. M., J. R. Stedinger, and R. P. Hooper (2003), Discharge indices for water quality loads, *Water Resour. Res.*, *39*(10), 1273, doi:10.1029/2002WR001872.

Wathen, S. J., R. I. Ferguson, T. B. Hoey, and A. Werritty (1995), Unequal mobility of gravel and sand in weakly bimodal river sediments, *Water Resour. Res.*, *31*(8), 2087–2096, doi:10.1029/95WR01229.

Wilcock, P. R., and J. C. Crowe (2003), Surface-based transport model for mixed-size sediment, *J. Hydraul. Eng.*, *129*(2), 120–128, doi:10.1061/(ASCE)0733-9429(2003)129:2(120).

Wilcock, P. R., and B. T. DeTemple (2005), Persistence of armor layers in gravel-bed streams, *Geophys. Res. Lett.*, *32*, L08402, doi:10.1029/2004GL021772.

Wilcock, P. R., S. T. Kenworthy, and J. C. Crowe (2001), Experimental study of the transport of mixed sand and gravel, *Water Resour. Res.*, *37*(12), 3349–3358, doi:10.1029/2001WR000683.

Williams, G. P. (1978), Bankfull discharge of rivers, *Water Resour. Res.*, *14*(6), 1141–1154, doi:10.1029/WR014i006p01141.

Wolman, M. G., and L. B. Leopold (1957), *River Flood Plains: Some Observations on Their Formation*, p. 30, U.S. Geol. Surv. Prof. Pap. 282-C, U.S. Govt. Print Off., Washington D. C.

Wolman, M. G., and J. P. Miller (1960), Magnitude and frequency of forces in geomorphic processes, *J. Geol.*, *68*(1), 54–74, doi:10.1086/626637.

Wong, M., and G. Parker (2006), One-dimensional modeling of bed evolution in a gravel bed river subject to a cycled flood hydrograph, *J. Geophys. Res.*, *111*, F03018, doi:10.1029/2006JF000478.

Zhou, Z., et al. (2017), Is "morphodynamic equilibrium" an oxymoron?, *Earth Sci. Rev.*, *165*, 257–267, doi:10.1016/j.earscirev.2016.12.002.